nature neuroscience

Esr1+ cells in the ventromedial hypothalamus control female aggression

Koichi Hashikawa[1,7], Yoshiko Hashikawa[1,7], Robin Tremblay[1], Jiaxing Zhang[2], James E Feng[1], Alexander Sabol[1], Walter T Piper[3], Hyosang Lee[4], Bernardo Rudy[1] & Dayu Lin[1,3,5,6]

As an essential means of resolving conflicts, aggression is expressed by both sexes but often at a higher level in males than in females. Recent studies suggest that cells in the ventrolateral part of the ventromedial hypothalamus (VMHvl) that express estrogen receptor-α (Esr1) and progesterone receptor are essential for male but not female mouse aggression. In contrast, here we show that VMHvl^{Esr1+} cells are indispensable for female aggression. This population was active when females attacked naturally. Inactivation of these cells reduced female aggression whereas their activation elicited attack. Additionally, we found that female VMHvl contains two anatomically distinguishable subdivisions that showed differential gene expression, projection and activation patterns after mating and fighting. These results support an essential role of the VMHvl in both male and female aggression and reveal the existence of two previously unappreciated subdivisions in the female VMHvl that are involved in distinct social behaviors.

Aggressive behavior is essential in competing for food, defending the home, protecting self and family, and enhancing overall survival opportunity in both sexes. In many species, mating opportunities are limited and therefore aggression is also used to compete for mates. As a result of natural selection[1], males in those species often express higher level of aggression[2]. Given that aggressive behaviors are far more prevalent in males in many vertebrates, including humans, most studies of the biological basis of aggression have focused on males. Early lesion and electrical stimulation studies identified the medial hypothalamus as a region essential for male aggression[3–5]. Recently, studies from our group and others have identified the VMHvl, a small subnucleus situated most ventrally in the medial hypothalamus, as a region essential for aggression in the male mouse[6–11]. In particular, optogenetically activating the VMHvl cells expressing Esr1 (whose expression overlaps nearly 100% with progesterone receptor (PR) expression) elicits immediate attack whereas optogenetic inactivation of the VMHvl^{Esr1+} cells or ablation of the VMHvl^{PR+} cells abolishes inter-male attack[6,9].

While one electrical stimulation study in rats suggested that male and female aggression involve similar medial hypothalamic regions[12], perturbing the VMHvl^{Esr1+} or VMHvl^{PR+} cells appeared to affect only male but not female aggression[6,9]. In addition, male but not female aggression was reduced either by knocking out the Esr1 gene in the whole animal[13] or by suppressing its expression specifically in the VMHvl using RNAi[14,15]. Instead, the VMHvl has a well-established role in promoting female sexual behavior[9,16–19]. Electrical stimulation of the VMHvl can facilitate lordosis in female rats in the absence of males[19]. Most compellingly, Esr1 knockdown or ablation of the VMHvl^{PR+} cells significantly reduces sexual receptivity but fails to reduce aggression in female mice[9,20]. These studies concluded that the Esr1$^+$PR$^+$ population in the VMHvl serves fundamentally different roles in female and male social behaviors: it mediates aggression in males but sexual behaviors in females[21–23].

Here we re-examined the role of the VMHvl in female aggression using a series of functional manipulation and recording tools. We found clear evidence supporting an essential role of the VMHvl^{Esr1+} cells in female aggression. Additionally, we discovered two previously unappreciated subdivisions in the female VMHvl, one for aggression and one for sexual behaviors.

RESULTS

Aggressive behaviors in laboratory female mice

Female aggression can differ widely based on females' reproductive state[24] and genetic background[25], and the opponent type[26]. Thus, we first tested the behaviors of female laboratory mice under a variety of resident–intruder conditions (**Supplementary Table 1**). We found that aggression could be reliably induced (defined as repeated attacks occurring in over 50% of subject mice) when (i) a virgin Swiss Webster (SW) female encountered a juvenile intruder of either sex in her home cage; (ii) a lactating SW female encountered any intruder; or (iii) a lactating C57 female encountered a juvenile intruder. We also noticed that some singly housed SW virgin females (6 of 10) briefly attacked a female intruder during their initial encounter (latency to final attack during the resident-intruder test (mean ± s.d.): 68.7 ± 43.1 s). Unexpectedly, 6 of 10 singly housed C57 females showed

[1]Neuroscience Institute, New York University School of Medicine, New York, New York, USA. [2]Department of Physiology, Medical College of Xiamen University, Xiamen, Fujian, China. [3]Center for Neural Science, New York University, New York, New York, USA. [4]Department of Brain and Cognitive Sciences, DGIST, Daegu, Korea. [5]Department of Psychiatry, New York University School of Medicine, New York, New York, USA. [6]Emotional Brain Institute, New York University School of Medicine, New York, New York, USA. [7]These authors contributed equally to this work. Correspondence should be addressed to D.L. (dayu.lin@nyumc.org).

Received 31 October 2016; accepted 17 August 2017; published online 18 September 2017; doi:10.1038/nn.4644

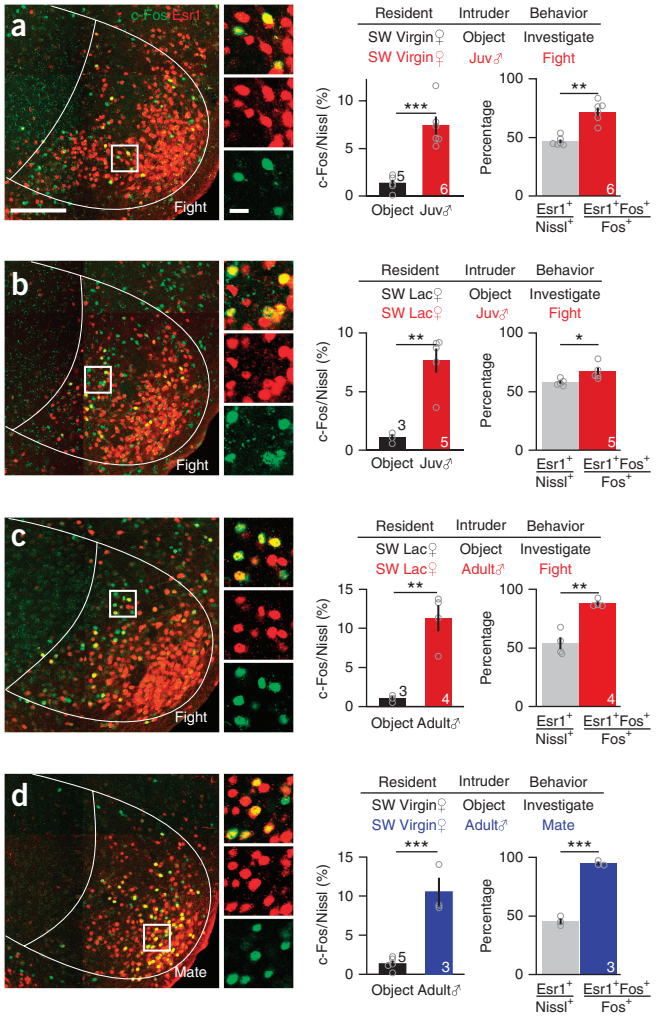

Figure 1 Esr1+ neurons in the VMHvl of female mice are preferentially activated during fighting and mating. (**a**–**d**) Left: representative images showing the expression of Esr1 (red) and c-Fos (green) in the VMHvl of (**a**) a virgin or (**b**) a lactating (Lac) female mouse that attacked a juvenile (Juv) male mouse, (**c**) a lactating female mouse that attacked an adult male mouse and (**d**) a virgin female mouse that mated with an adult male. Insets show the boxed areas. Scale bars: 150 µm (left) and 20 µm (insets). Middle: the percentage of neurons in the VMHvl that expressed c-Fos after various stimulus conditions. Unpaired *t*-test. Right: the percentage of Esr1+ neurons in all VMHvl neurons (gray) and the percentage of c-Fos+ neurons expressing Esr1 in the VMHvl after fighting (red) or mating (blue). Paired *t*-test. $^{*}P < 0.05$, $^{**}P < 0.01$, $^{***}P < 0.001$. Data are presented as means ± s.e.m. Number of mice *N* for each group is indicated on the bar. See **Supplementary Table 2** for detailed statistics. See also **Supplementary Figure 1**.

male-style mounting toward female intruders and, to a lesser extent, toward juveniles.

VMHvl^{Esr1+} cells are highly active during female aggression and sexual behaviors

Using the aggression-inducing conditions that we identified, we found that VMHvl consistently expressed high levels of c-Fos, a surrogate marker of neural activity, after aggression in both virgin and lactating females (**Supplementary Fig. 1**). The number of c-Fos+ cells in the VMHvl was significantly larger in lactating females that attacked the adult male than those that did not, suggesting that VMHvl activation is at least partially due to the expression of aggression (**Supplementary Fig. 1**). Motivated by the high level of female aggression-induced c-Fos in the VMHvl, we pharmacogenetically inactivated the VMHvl in wild-type SW lactating females and found significantly reduced aggression, supporting an essential role of the VMHvl in female aggression (**Supplementary Note 1** and **Supplementary Fig. 2**).

We next asked whether female aggression-activated VMHvl cells preferentially overlap with the Esr1+ cells, as previously observed in males[6]. Whereas approximately 50% of VMHvl neurons expressed Esr1, 60–80% of fighting-induced c-Fos-positive cells expressed Esr1 (**Fig. 1a–c**). This preferential overlap between Esr1 and fighting-induced c-Fos suggests that VMHvl^{Esr1+} cells may be a relevant population for female aggression. Consistent with a well-known role of VMHvl cells, especially those that express Esr1+, in female sexual behaviors[9,16–20,27], mating induced abundant c-Fos expression in the VMHvl and over 90% of mating-induced c-Fos+ cells expressed Esr1 (**Fig. 1d**).

To directly observe the activity of the VMHvl^{Esr1+} cells during female aggression and mating, we recorded the activity of VMHvl^{Esr1+} cells in freely moving mice using fiber photometry[8,28,29] (**Fig. 2a**). We virally expressed a genetically encoded fluorescent calcium sensor, GCaMP6f[30], and a control fluorophore, mCherry, in the VMHvl of *Esr1-2A-Cre* SW mice[6] and implanted a 400-µm optic fiber above the injection site (**Fig. 2b,c**). Histological analysis revealed that 94.2 ± 2.0% of cells under the light cone were within the VMHvl. During the recording session, we sequentially introduced an adult male, a juvenile male or an object into the home cage of the recorded female in pseudorandomized order, each for 15–20 min. During object investigation or general locomotion, the GCaMP6f signal did not change (**Fig. 2d** and **Supplementary Video 1**). When a virgin female investigated or attacked a juvenile, or investigated or was mounted by a male, GCaMP6f activity increased acutely. The response magnitudes during attack and mating were similar (**Fig. 2e,f,j** and **Supplementary Videos 2** and **3**). When a lactating female investigated or attacked a juvenile or male intruder, GCaMP6f activity also increased. The magnitude of response during attacks on adult males was higher than that during attacks on juvenile males (**Fig. 2g,h,k** and **Supplementary Video 4**; $\Delta F/F$: attack juvenile, 8.0 ± 2.3%; attack adult male, 15.1 ± 2.4%, $P = 0.040$, paired *t*-test, $N = 6$ mice). Activity change was minimal when a lactating female investigated or retrieved her own pup (**Fig. 2i**). GCaMP6 signal also increased during investigation of urine. Adult male urine elicited larger responses than juvenile urine in lactating females but comparable responses in virgin females (**Supplementary Fig. 3**). Despite the clear VMHvl response while investigating intruders and their associated odors, the signal increase during attack cannot be simply accounted by the olfactory inputs for two reasons. First, the GCaMP6f responses during attack-only trials (attack not followed or preceded by investigation) were significantly larger than the responses during investigation-only trials (investigation not followed or preceded by attack) (**Fig. 2l**). Second, GCaMP6 responses were similar during attack trials that were preceded by investigation and those that were not (attack with preceding investigation toward a juvenile in lactating females: 8.7 ± 2.7%; attack only: 8.5 ± 2.6%; $P = 0.88$, paired *t-test*). Furthermore, we noted that the responses during investigation were modulated by the level of aggression. The response during investigation was larger when it was followed by attack than when it was not (**Fig. 2m**). The response during investigation-only trials was significantly larger on days during which the juvenile intruder was attacked at least once than on no-attack days in virgin females (**Fig. 2n**).

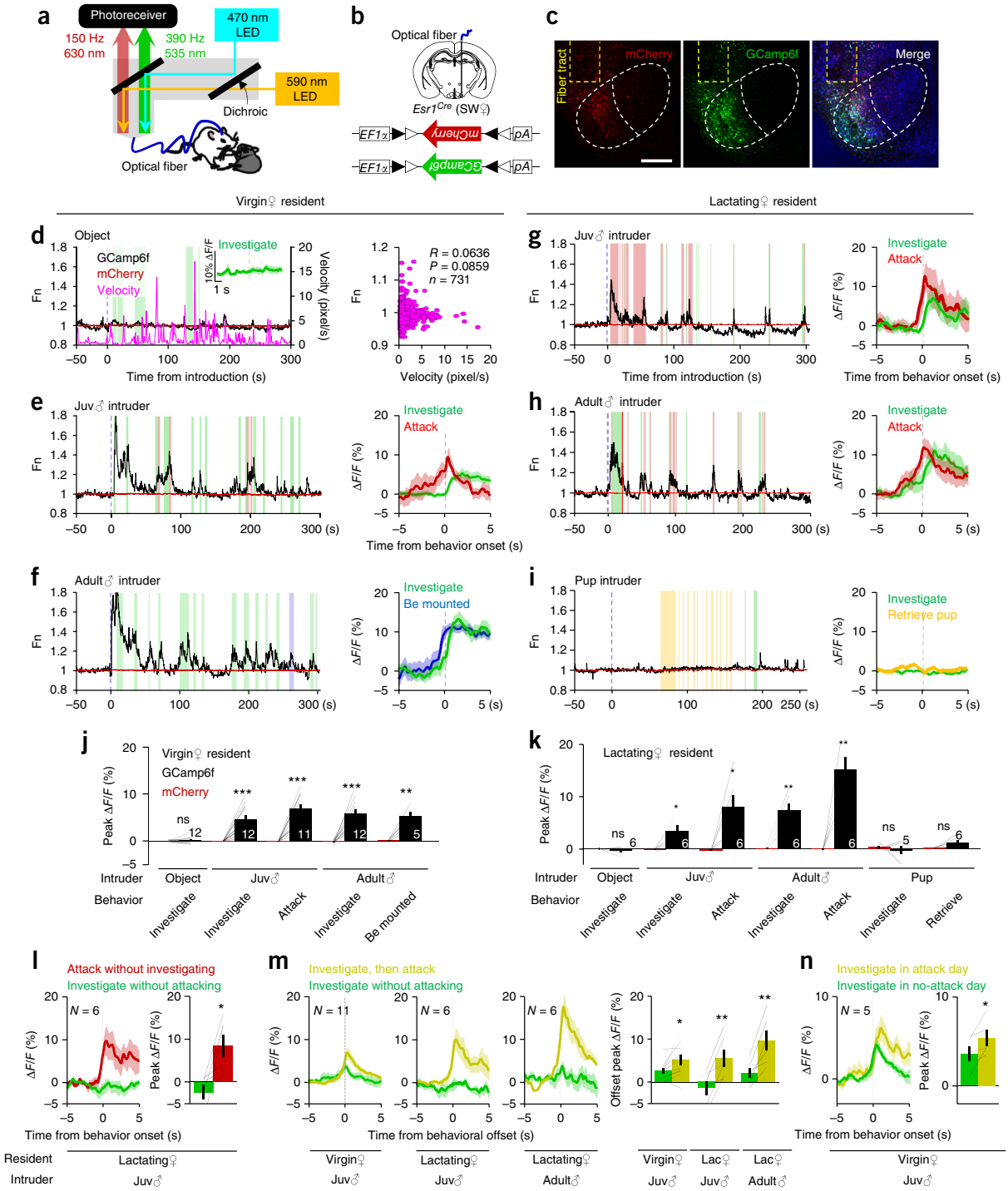

Figure 2 Responses of the Esr1+ population in the female VMHvl during fighting and mating. (**a**) Light paths for fiber photometry recording. (**b**) Viral constructs and implantation scheme. (**c**) Representative images showing mCherry (red), GCaMP6f (green), Nissl (blue) and optical fiber tract (yellow dashed line). Scale bar: 300 μm. (**d**–**i**) Left: representative normalized GCaMP6f (black) and mCherry (red) traces during interaction with (**d**) an object and (**e**–**i**) various social stimuli introduced into the home cage of the test female. Colored shading marks behavioral episodes. Green: investigation; blue: being mounted; red: attack, yellow: pup retrieval. Fn, normalized fluorescence. (**d**) Right: the velocity of the recorded animal did not correlate with GCaMP6f signal. Pearson product-moment correlation. Inset in **d** and right panels in **e**–**i** show representative peri-event time histograms (PETHs) of GCaMP6f signal aligned to the onset of various behaviors. (**j**,**k**) The peak $\Delta F/F$ of GCaMP6f (black) and mCherry (red) signals during various behaviors in virgin (**j**) and lactating (**k**) females. (**l**–**n**) Population PETHs (left) and the peak $\Delta F/F$ (right) of GCaMP6f signals aligned to the onset (**l**,**n**) or offset (**m**) of various behaviors. **j**–**n**: paired *t*-test. $^{*}P < 0.05$, $^{**}P < 0.01$, $^{***}P < 0.01$. Data are presented as means ± s.e.m. *N* is the number of mice; *n* is the number of cells. See **Supplementary Table 2** for detailed statistics. See also **Supplementary Figures 3**–**5**.

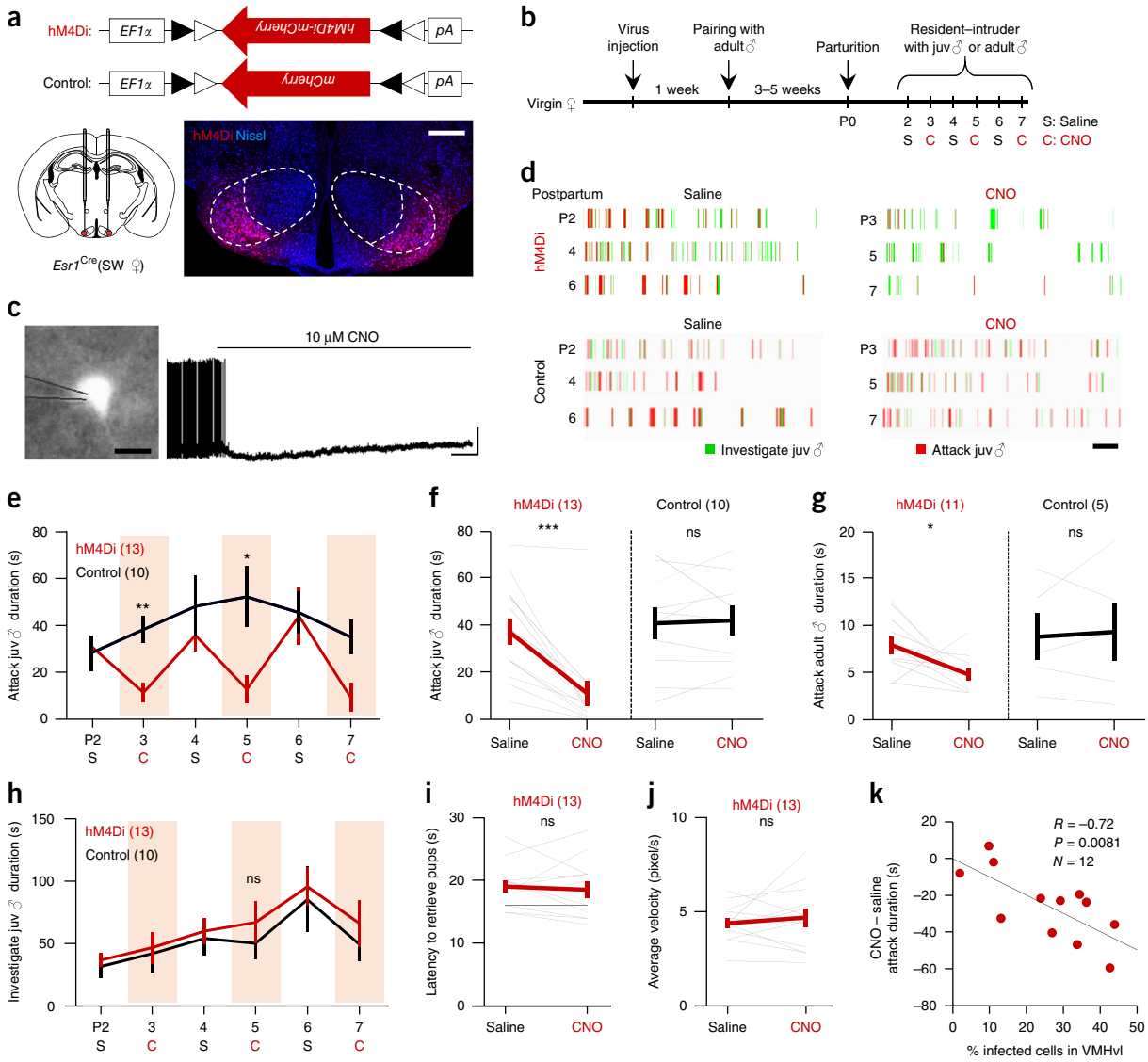

Figure 3 The activity of Esr1+ neurons in the VMHvl is necessary for female aggression. (**a**) Viral constructs and a representative histological image showing the expression of hM4Di-mCherry (red) at the injection sites. Scale bar: 300 μm. (**b**) Experimental schedule. (**c**) Left: *in vitro* whole-cell patch clamp recording from a representative Esr1+ neuron from the VMHvl (scale bar: 10 μm). Right: changes in the cell's spontaneous spiking activity after application of 10 μM CNO. Horizontal and vertical scale bars: 30 s and 20 mV. The result was replicated in two hM4Di-mCherry–expressing cells. (**d**) Behavioral results for representative test and control animals. Scale bar: 60 s. (**e**) Reduction in aggression was reproduced on multiple CNO injection days. (**f**,**g**) Attack durations toward (**f**) juvenile male and (**g**) adult male intruders were significantly decreased after CNO injection in the hM4Di group but not in the control mCherry group. (**h**–**j**) No significant change was observed in (**h**) duration of investigation of a juvenile male intruder, (**i**) the time spent to retrieve four scattered pups and (**j**) the average movement velocity in the hM4Di group after CNO injection in comparison to saline injection. **e**–**j** only include animals with over 10% of infected cells in the VMHvl. (**k**) The percentage of cells that were infected in the VMHvl was significantly correlated with the magnitude of the decrease in attack duration toward a juvenile male intruder after CNO injection. **k** includes all animals with attack duration over 20 s on saline days regardless of the percentage of infected cells. (**e**,**h**) Two-way repeated measure ANOVA followed by Holm–Sidak *post hoc* multiple comparisons. (**f**,**g**,**i**,**j**) Paired *t*-test. (**k**) Pearson product-moment correlation. $^{*}P < 0.05$, $^{**}P < 0.01$, $^{***}P < 0.001$. Data are presented as means ± s.e.m. See **Supplementary Table 2** for detailed statistics. See also **Supplementary Figure 6**.

In C57 female mice, we observed qualitatively similar responses during investigation, mating and attack (**Supplementary Fig. 4**). In all animals, the simultaneously recorded mCherry signal was not significantly modulated during any of these behaviors (**Fig. 2d–k** and **Supplementary Fig. 5**). Together these data show that VMHvl^{Esr1+} cells in females are highly active during aggression and sexual behaviors, but not maternal behaviors.

VMHvl^{Esr1+} cells are necessary for female aggression

To test whether VMHvl^{Esr1+} cells are necessary for female aggression, we virally expressed hM4Di-mCherry in the VMHvl^{Esr1+} cells of *Esr1-2A-Cre* SW virgin female mice (**Fig. 3a**,**b**). For one group of animals, 1 week after viral injection, we paired each female with an adult male mouse until midterm pregnancy, and conducted resident–intruder tests between postpartum days 2 and 7. A second group of virgin

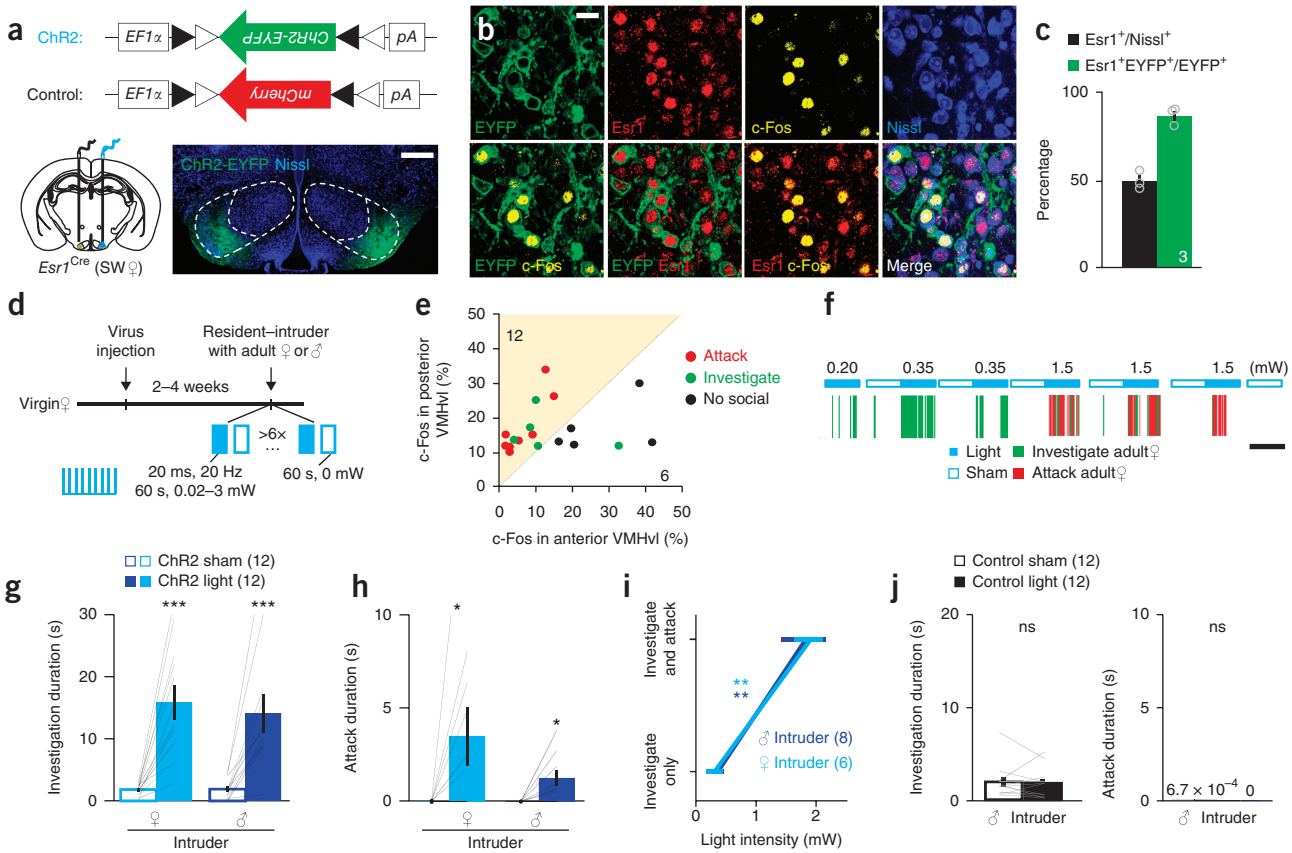

Figure 4 Activation of the Esr1+ neurons in the VMHvl is sufficient to induce attack in virgin female mice. (**a**) Viral constructs and a histological image showing ChR2-EYFP expression (green) at the injection sites. Scale bar: 300 μm. (**b**) Images showing the expressions of ChR2-EYFP (green), Esr1 (red), c-Fos (yellow), Nissl (blue) and their overlaps. Scale bar: 20 μm. (**c**) The percentage of all VMHvl neurons expressing Esr1 (black) and the percentage of ChR2-EYFP+ neurons expressing Esr1 (green). (**d**) Experimental schedule. (**e**) The percentage of VMHvl cells expressing light-induced c-Fos in the anterior vs. posterior VMHvl of all tested sites with over 10% of light induced c-Fos. (**f**) Representative raster plots illustrating progressive behavioral changes toward a female intruder with increased light intensity. Scale bar: 60 s. (**g**,**h**) Increase in (**g**) duration of investigation and (**h**) duration of attack toward an adult female or male intruder during light-on period in comparison to sham-on period in animals with preferential posterior VMHvl activation. (**i**) The minimal light intensity that is required to elicit close investigation is lower than that to elicit attack against either a male or a female intruder. (**j**) The duration of investigation (left) and attacks (right) did not differ during light-on and sham-on periods in the control group. (**g**,**h**,**j**) Paired *t*-test. (**i**) Two-way repeated measure ANOVA followed by Holm–Sidak *post hoc* multiple comparisons. $^{*}P < 0.05$, $^{**}P < 0.01$, $^{***}P < 0.001$. Data are presented as means ± s.e.m. See **Supplementary Table 2** for detailed statistics. See also **Supplementary Figures 7–10**.

females were not paired with males and were tested 3 weeks after viral injection (**Supplementary Fig. 6a–e**).

During testing, we injected saline or clozapine-*N*-oxide (CNO, the engineered ligand for hM4Di)[31,32] intraperitoneally on interleaved days. *In vitro* whole-cell recordings from VMHvl brain slices confirmed that CNO suppressed the activity of hM4Di-mCherry–expressing cells (**Fig. 3c**). Thirty minutes after CNO injection, we introduced a male (for the lactating group) or a juvenile (for both lactating and virgin groups) into the home cage of the test animal for 10 min. CNO injection significantly and reproducibly reduced attack duration and frequency in the tested females regardless of their reproductive stage (**Fig. 3d–g** and **Supplementary Fig. 6c,d**). Social investigation, retrieval of the subject's own pups and locomotion were not affected by CNO injection (**Fig. 3h–j** and **Supplementary Fig. 6e**). The suppression of aggression was significantly correlated with the percentage of VMHvl cells expressing hM4Di-mCherry, such that animals with higher percentages of infected neurons showed more decrease in aggression after CNO injection (**Fig. 3k**). Control animals that expressed mCherry in the VMHvl^{Esr1+} cells showed no change in aggression after CNO injection (**Fig. 3e–g**). Additionally, in lactating *Esr1-2A-Cre* mice with a C57 background, inhibiting VMHvl^{Esr1+} cells nearly abolished aggression against juvenile intruders (**Supplementary Fig. 6f–j**). Thus, VMHvl^{Esr1+} cells are necessary for female aggression regardless of reproductive stage and genetic background.

VMHvl^{Esr1+} cells are sufficient to drive female aggression

We next tested whether VMHvl^{Esr1+} cells are sufficient to elicit aggression in females by virally expressing ChR2-EYFP[33] in VMHvl^{Esr1+} cells of *Esr1-2A-Cre* SW mice (**Fig. 4a**). Approximately 90% of ChR2-EYFP–expressing cells were Esr1+ (**Fig. 4b,c**). We delivered blue light unilaterally to the VMHvl when the virgin female encountered an adult male or female intruder, two conditions with minimal natural aggression (**Fig. 4d**). Light induced an increase in social investigation and attack in a subset of subjects. *Post hoc* histology revealed that attack and investigation were predominantly induced from stimulation sites that expressed more light-induced c-Fos in the posterior (from bregma: −1.6 to −2.0 mm) than the anterior (from bregma: −1.4 mm) VMHvl (**Fig. 4e**). Eight out of 12 posteriorly biased VMHvl sites (8 animals; see Online Methods) elicited attack and all 12 sites

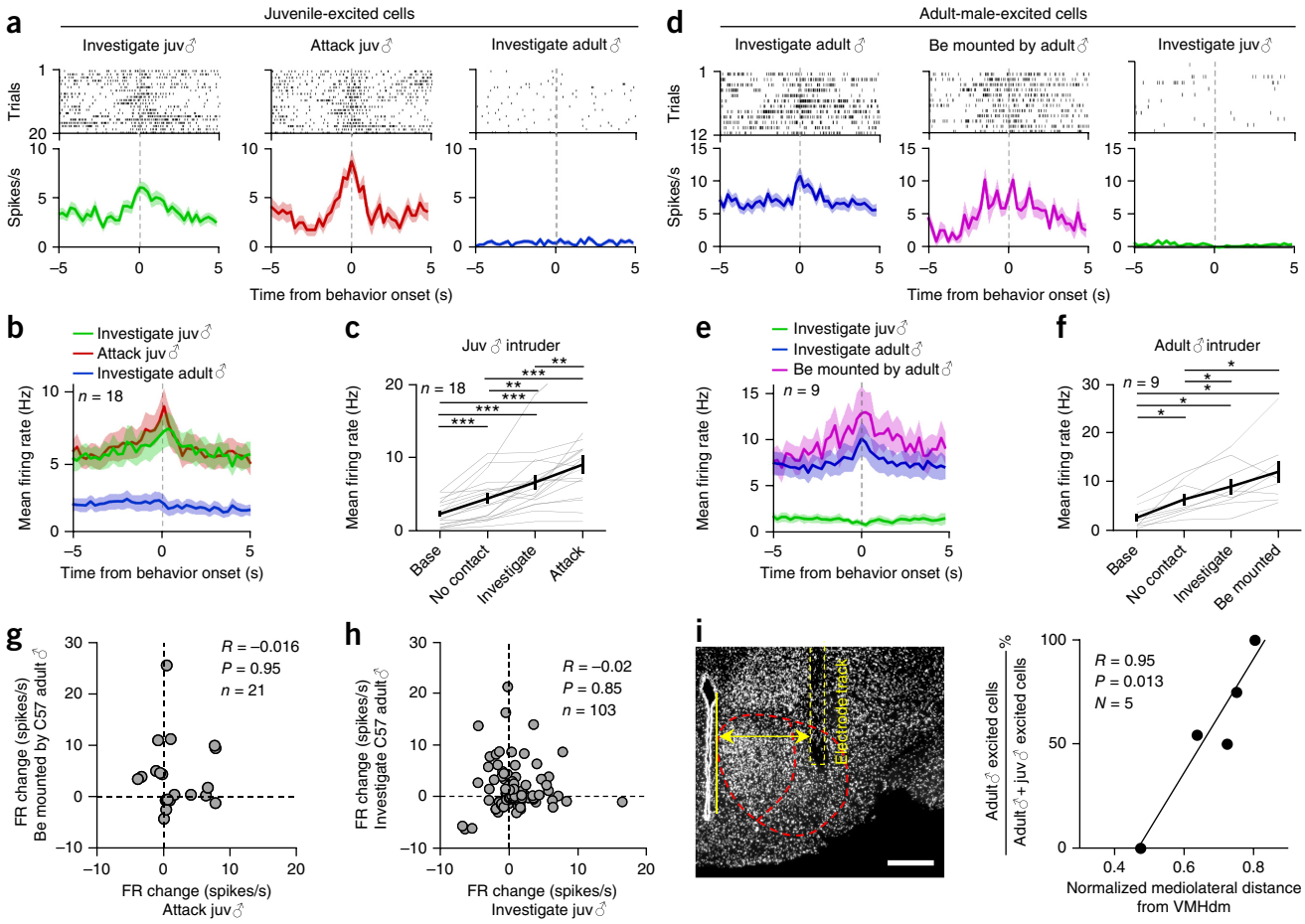

Figure 5 Electrophysiological responses of female VMHvl neurons during encounters with adult male and juvenile intruders. (**a**) Raster plots (top) and PETHs (bottom) aligned to the onsets of various behavioral episodes for a juvenile-excited cell. (**b**) Average PETHs of the firing rate from 18 juvenile-excited cells. (**c**) Firing rates of juvenile-excited cells before juvenile introduction (base) and when the animal investigated, attacked or stayed away from (no contact) the juvenile. **b** and **c** only show the subset of juvenile-excited cells with episodes of attack on the juvenile (> 3 s). (**d**) Example and (**e**,**f**) population responses of adult-male-excited cells. Figure conventions as in **a**–**c**. **d**–**f** only show the subset of male-excited cells with episodes of being mounted (>3 s). (**g**,**h**) Distributions of the firing rate (FR) changes (**g**) during attack and being mounted or (**h**) during investigation of a juvenile and investigation of an adult male across all the recorded cells with both behaviors. (**i**) Left, a representative histological image showing the electrode track. Scale bar: 300 µm. Right, the correlation between mediolateral position of the electrode and the percentage of recorded male-excited cells among all male-excited and juvenile-excited cells. (**c**,**f**) One-way ANOVA followed by Holm–Sidak *post hoc* multiple comparisons. (**g**–**i**) Pearson product-moment correlation. $^{*}P < 0.05$, $^{**}P < 0.01$, $^{***}P < 0.001$. Data are presented as means ± s.e.m. See **Supplementary Table 2** for detailed statistics. See also **Supplementary Figure 11**.

elicited investigation. In contrast, none of the 6 anteriorly biased sites (4 animals) induced attack and only one site induced investigation (**Fig. 4e** and **Supplementary Fig. 7**). In those posterior VMHvl-biased animals, low-intensity light (20 ms, 20 Hz, 0.34 ± 0.078 mW) significantly increased only investigation (**Fig. 4f**,**g** and **Supplementary Video 5**), while higher intensity light (20 ms, 20 Hz, 1.86 ± 0.23 mW) elicited both investigation and attack (**Fig. 4f**,**h**,**i** and **Supplementary Video 5**). Control SW females that expressed mCherry in the VMHvl^{Esr1+} cells showed no change in investigation or attack during light delivery (**Fig. 4j**).

One study found that optogenetic activation of VMHvl^{Esr1+} cells in C57 virgin females induces social investigation and mounting but not aggression[6]. We attempted to reconcile our results with the previous study by optogenetically activating the VMHvl^{Esr1+} cells in C57 females using the conditions identical to those for SW females. Consistent with the previous report[6], we observed light-induced social investigation and mounting but no attack (**Supplementary Fig. 8a**–**e**). The mounting was induced upon light stimulation and occurred against both natural (for example, female) and unnatural (for example, male) social targets (**Supplementary Fig. 8e** and **Supplementary Video 6**). In support of a role of the female VMHvl in driving mounting, both c-Fos staining and fiber photometry recording revealed increased activity in the VMHvl upon natural female-female mounting (**Supplementary Fig. 8f**,**g**). In contrast to virgin C57 females, lactating C57 females that naturally attacked intruders were induced to attack by all posteriorly biased stimulation sites (**Supplementary Fig. 9** and **Supplementary Video 7**).

Previous studies have suggested a correlation between aggression in lactating female rats and anxiety[34]. To test the possibility that our activation-induced attack was due to a change in anxiety, we activated the aggression-inducible VMHvl sites in an elevated plus maze. We observed no significant differences in the amount of time animals spent in the open arm during pre-stimulation, light-on, sham-on (0 mW) and post-stimulation periods (**Supplementary Fig. 10**). Thus, VMHvl^{Esr1+} cells were able to drive both aggression and male-style mounting in female mice. The exact form of light-induced behavioral

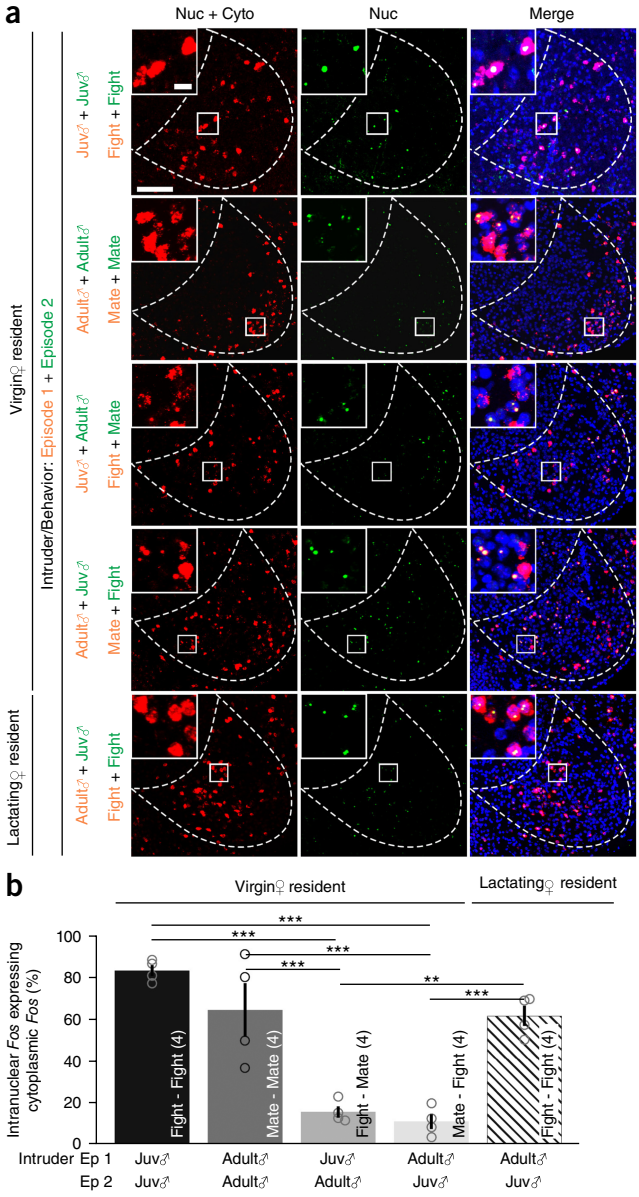

Figure 6 Topographical organization of fighting- and mating-related cells in the female VMHvl. (**a**) Cytoplasmic (Cyto) + nuclear (Nuc) (red) and nuclear only (green) *Fos* induced by two sequential behavioral episodes. Insets show enlarged images of the boxed areas. Blue: Hoechst. Scale bars: 150 µm (main panels) and 20 µm (insets). (**b**) Percentage of neurons expressing nuclear *Fos* that also express cytoplasmic *Fos*. One-way ANOVA followed by Tukey's multiple comparisons. $^{**}P < 0.01$, $^{***}P < 0.001$. Data are presented as means ± s.e.m. See **Supplementary Table 2** for detailed statistics. See also **Supplementary Figure 12**.

change followed the pattern of natural social behaviors determined by the animals' genetic background and reproductive state.

Distinct fighting- and mating-related cells in female VMHvl

The VMHvl^{Esr1+} cells are clearly essential for both female aggression and sexual behaviors[9,16–20]. How do the mating- and aggression-excited cells relate to each other? To address this question, we performed electrophysiological recordings in freely moving virgin SW female mice[7,8,10,35,36]. A total of 103 single units were recorded from five females. Among them, 22 cells were juvenile-excited. They significantly increased firing rate while the female was investigating and/or attacking a juvenile (**Fig. 5a–c**). The increase in firing was higher during attack than investigation (**Fig. 5c**). Twenty-seven cells were adult male excited. They significantly increased firing rate while the female was investigating an adult male and/or being mounted (**Fig. 5d–f**). Only 4 cells were excited by both males and juveniles. Another 4 cells were suppressed during these interactions. As a population, the juvenile-excited cells did not change firing rate during male interaction and the male-excited cells were weakly suppressed during juvenile interaction (**Supplementary Fig. 11a,b**). Across all 103 cells, there was no correlation between the firing rate changes during attacking and mating (**Fig. 5g**), or during investigating juveniles and investigating males (**Fig. 5h** and **Supplementary Fig. 11c**), whereas the responses during investigating males of different strains or responses during investigating juvenile males and females were significantly correlated (**Supplementary Fig. 11d,e**). Thus, two largely distinct subpopulations, one for mating and one for fighting, exist in the female VMHvl.

In our five recorded animals, we noted that the juvenile-excited and adult-male-excited cells were not distributed evenly. In the animal with the most laterally positioned electrode bundle, only male-excited cells (8 of 11 recorded cells) were recorded. In contrast, in the animal with the most medially positioned electrode, only juvenile-excited cells (6 of 29 cells) were recorded. In the remaining three animals, with electrodes centrally located in the VMHvl, both juvenile- and male-excited cells were recorded (**Fig. 5i**).

Topographical organization of fighting- and mating-related cells in female VMHvl

To further understand the spatial distribution of fighting- and mating-related neurons in the VMHvl, we performed a side-by-side comparison of c-Fos induced by mating and fighting. We observed a clear difference. Fighting, regardless of the reproductive state of the female and the type of intruder, invariably induced dense c-Fos expression in the medial part of the VMHvl whereas the mating-induced c-Fos$^+$ cells were more laterally located (**Supplementary Fig. 12a–c**). To quantify this difference, we measured the position of each c-Fos$^+$ cell in the VMHvl. While fighting- and mating-induced c-Fos$^+$ cells were located at the similar medial–lateral level in the anterior VMHvl, the fighting-induced c-Fos$^+$ cells were significantly more medially located than the mating-induced c-Fos in the posterior VMHvl (**Supplementary Fig. 12a–c**). Consistent with a more important role of the posterior VMHvl in female aggression, more c-Fos$^+$ cells were found at the posterior VMHvl than the anterior VMHvl after female aggression while c-Fos$^+$ cells induced by female mating were uniformly distributed along the anterior–posterior axis (**Supplementary Fig. 12d,e**).

To compare mating- and fighting-induced c-Fos expression in the same animal, we used *Fos* cellular compartment analysis of temporal activity by fluorescence *in situ* hybridization (catFISH)[7,37]. Mating- and fighting-induced *Fos* were clearly topographically organized (**Fig. 6a**). Detailed cell counting revealed that in virgin females that experienced fighting or mating twice, approximately 70% of cells expressed both intranuclear and cytoplasmic *Fos* in VMHvl (**Fig. 6a,b**). Lactating females that sequentially attacked an adult male and a juvenile intruder also showed high overlap between intranuclear and cytoplasmic *Fos* (**Fig. 6a,b**). In contrast, when the female fought and then mated, or mated and then fought, only 10% of intranuclear and cytoplasmic *Fos* overlapped (**Fig. 6a,b** and **Supplementary Video 8**). These results indicate, first, that the same neurons are likely to be recruited during two successive episodes of the same social behavior, regardless of the type

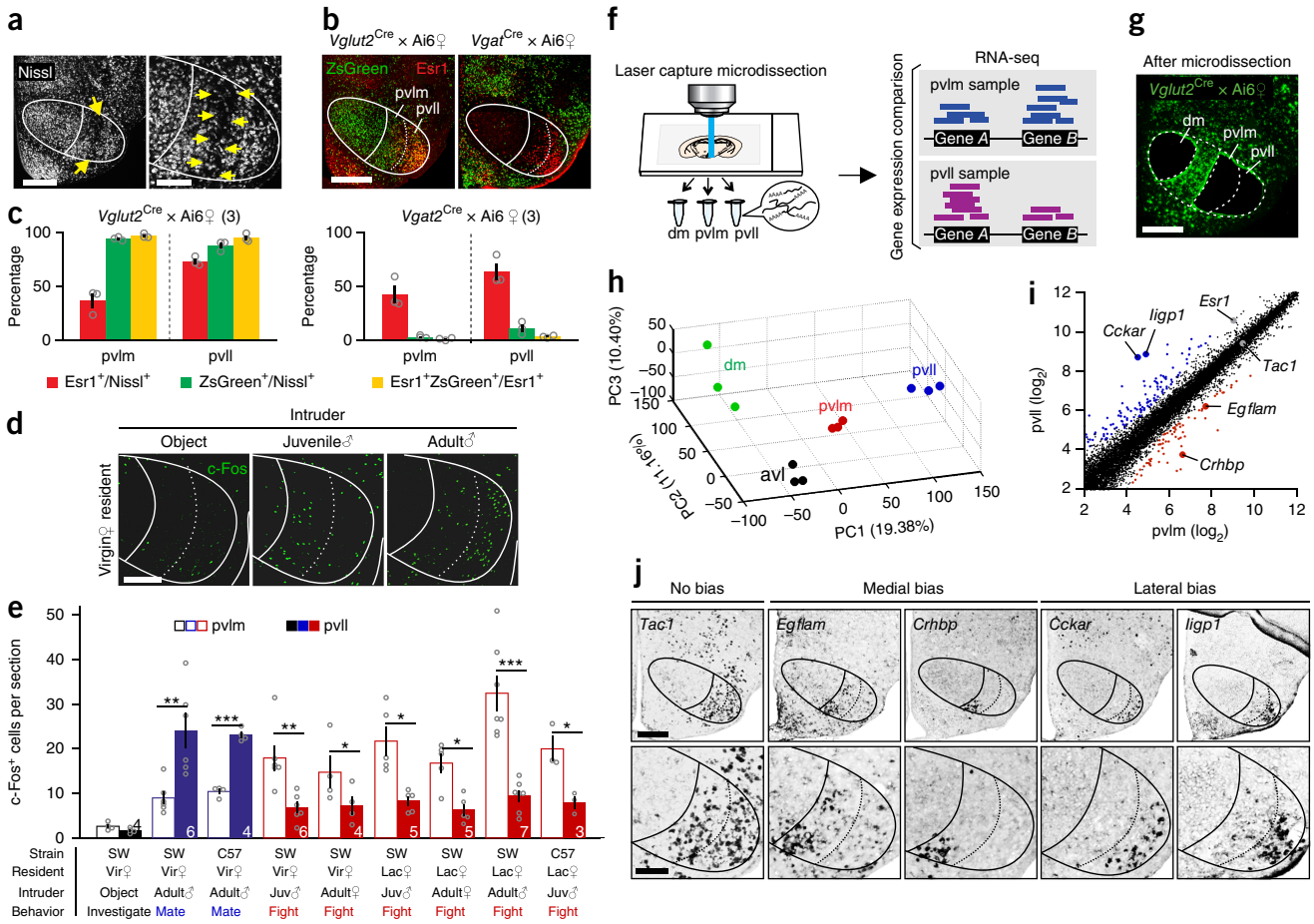

Figure 7 Female VMHvl has anatomically and molecularly distinct subdivisions. (**a**) Nissl staining illustrating the boundary (yellow arrows) between female VMHpvlm and VMHpvll. Scale bars (left and right, respectively): 300 and 150 μm. (**b**) Overlay of Esr1 (red) and ZsGreen (green; ZsGreen1, enhanced green fluorescent protein) in the VMHvl of a female *Vglut2-ires-Cre* × Ai6 mouse (left) and a female *Vgat-ires-Cre* × Ai6 mouse (right). Scale bar: 300 μm. (**c**) The percentage of Esr1+ (red), Vglut2+ (green, left) and Vgat+ (green, right) cells in the VMHpvll and VMHpvlm and the percentage of Esr1+ cells that overlap with Vglut2+ or Vgat+ cells (yellow). $N = 3$ animals for each group. (**d**) Object investigation-induced, fighting-induced or mating-induced c-Fos (green) in the VMHvl in virgin female mice. Scale bar: 150 μm. (**e**) Average number of c-Fos+ cells per section in the VMHpvlm and VMHpvll following object investigation (black), fighting (red) or mating (blue) in female mice. $N = 3$–7; paired *t*-test. $^*P < 0.05$, $^{**}P < 0.01$, $^{***}P < 0.001$. (**f**) Experimental scheme. (**g**) A brain section from a *Vglut2-ires-Cre* × Ai6 mouse after microdissection of VMHdm, VMHpvll and VMHpvlm. Scale bar: 300 μm. (**h**) RNA-seq results for all samples from various VMHvl subregions mapped onto the principal component (PC) space. (**i**) Average normalized counts of each gene in the VMHpvlm (*x* axis) and VMHpvll (*y* axis). Red and blue dots represent genes with significantly biased expression (Benjamini and Hochberg method, $P < 0.05$, >1.2×, $\log_2$ scale). (**j**) *In situ* hybridization in the VMHvl for five of the genes indicated in **i**. Scale bars (top and bottom, respectively): 300 and 150 μm. Data are presented as means ± s.e.m. See **Supplementary Table 2** for detailed statistics. See also **Supplementary Figure 13**.

of intruder; and second, that female mating and fighting recruit largely distinct sets of neurons in spatially segregated regions of the VMHvl.

The female VMHvl contains two molecularly distinguishable subregions

The distinct *Fos* expression patterns after fighting and mating suggest that the female VMHvl may contain previously unappreciated compartments. We carefully examined pan-neuronal staining and noticed a cell-poor region within the posterior VMHvl that readily separates the area into a medial and a lateral zone (VMHpvlm and VMHpvll) (**Fig. 7a** and **Supplementary Fig. 13**). Visualization of glutamatergic neurons using *Vglut2-ires-Cre* × Ai6 mice[38,39] and of GABAergic neurons using *Vgat-ires-Cre* × Ai6 mice[38,39] supported the idea that the VMHpvlm and pvll were distinct from the surrounding nuclei, including the tuberal nucleus and lateral hypothalamus. Whereas those surrounding nuclei contained dense GABAergic neurons, as previously reported[40,41], VMHpvlm and VMHpvll were largely (>90%) occupied by glutamatergic neurons and Esr1+ cells were nearly exclusively glutamatergic (**Fig. 7b,c** and **Supplementary Fig. 13**). As expected, the fighting-induced c-Fos was mainly in the VMHpvlm whereas the mating-induced c-Fos was mostly in the VMHpvll (**Fig. 7d,e**).

If the VMHpvll and VMHpvlm are distinct brain structures, they likely also differ in their gene expression patterns[42]. Indeed, we noticed that Esr1 was expressed in fewer cells and at a lower intensity in the VMHpvlm than in the VMHpvll (Esr1+ percentage in VMHpvlm: 39.9 ± 4.8%; VMHpvll: 68.5 ± 4.2%; $P = 0.0125$, $N = 6$ animals; average intensity of Esr1 staining of VMHpvll cells divided by that of VMHpvlm cells: 1.86 ± 0.24, $P = 0.037$, $N = 4$ animals, *t*-test). To understand the genetic differences between the VMHpvlm and VMHpvll comprehensively, we performed RNA-seq using tissues dissected from VMHpvlm, VMHpvll, the anterior VMHvl (VMHavl), and dorsomedial VMH (VMHdm) in *Vglut2-ires-Cre* × Ai6 mice[43] (**Fig. 7f,g**). Principal

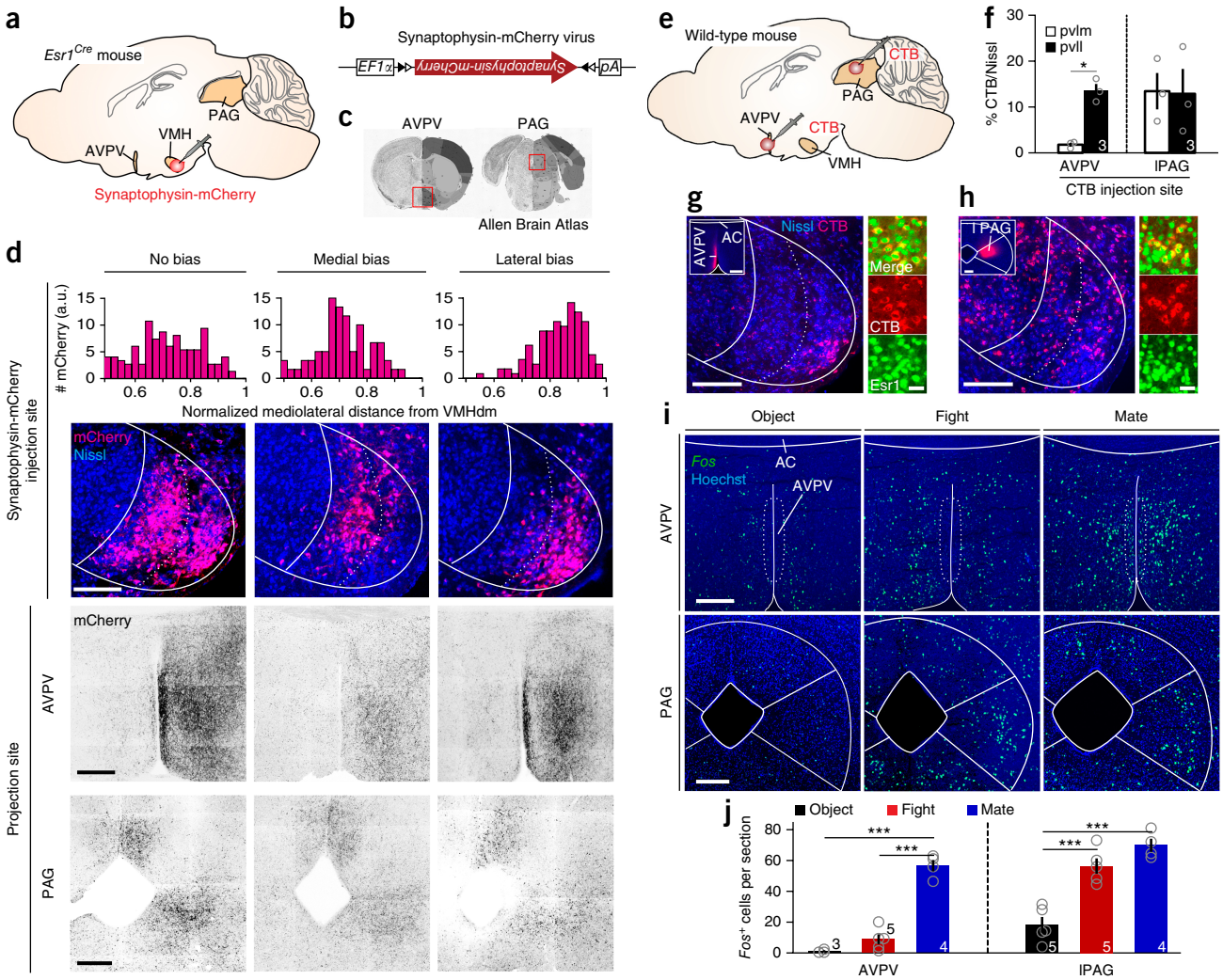

Figure 8 VMHpvlm and VMHpvll in female mice have distinct downstream targets. (**a**,**b**) Experimental scheme for anterograde tracing. (**c**) The two projection sites of the VMHvl (red boxes) that are shown in **d**. Images from Allen Brain Atlas. (**d**) Projection patterns in the AVPV and PAG in animals with primary infection in the whole VMHvl (left), VMHpvlm (middle) and VMHpvll (right). Scale bars (top to bottom): 150, 300 and 300 μm. Top bar graphs show the distributions of infected neurons in the VMHvl along the medial–lateral axis. (**e**) Experimental scheme of retrograde tracing. (**f**) Percentage of neurons in the VMHpvlm or VMHpvll that were retrogradely labeled from AVPV (left) or PAG (right). Paired *t*-test. $^*P < 0.05$. (**g**,**h**) Left large image shows neurons in the VMHvl that are retrogradely labeled (red) from (**g**) AVPV or (**h**) PAG. Insets show the injection sites. Scale bars: 150 μm (main panel) and 300 μm (inset). Right images show the overlap between the CTB labeling (red) and Esr1 (green). Scale bar: 20 μm. (**i**) *Fos* mRNA expression in the AVPV or PAG after various testing conditions. Scale bars: 300 μm. (**j**) Average number of *Fos*-expressing cells per section in the AVPV (left) and PAG (right) after various testing conditions. One-way ANOVA followed by Tukey's multiple comparisons. $^{***}P < 0.001$. Data are presented as means ± s.e.m. See **Supplementary Table 2** for detailed statistics. See also **Supplementary Figure 14**.

component analysis revealed that samples from the same VMH region were clustered in the principal component space and apart from samples from other regions (**Fig. 7h**). We found 74 genes enriched in the VMHpvlm and 126 in the VMHpvll (**Fig. 7i** and **Supplementary Data Set 1**). Of note, while most VMHpvll-enriched genes expressed differentially in VMHdm (107 of 126, $\log_2$ ratio > 1.2), only a small fraction of VMHpvlm-enriched genes were differentially expressed in the VMHdm (10 of 74, $\log_2$ ratio > 1.2).

Consistent with the Esr1 staining results, *Esr1* mRNA had significantly higher copy number in the VMHpvll than the VMHpvlm ($P < 0.01$, **Fig. 7i**). We further validated the RNA-seq results with *in situ* hybridization. Consistent with the RNA-seq data, *Cckar* and *Iigp1* were nearly exclusively expressed in the VMHpvll; *Crhbp* and *Egflam* were largely confined to the VMHpvlm while *Tac1* was expressed at high levels in both VMHvl regions (**Fig. 7j**). These data support the existence of molecularly distinguishable medial and lateral subdivisions in the female posterior VMHvl.

Visualization of targets downstream from the female VMHvl

Lastly, we investigated the projection patterns of the VMHpvll and VMHpvlm by stereotaxically injecting a small amount (15 nl) of an AAV expressing Cre-dependent synaptophysin-mCherry[44] into the VMHvl of *Esr1-2A-Cre* virgin SW female mice (**Fig. 8a–c** and **Supplementary Fig. 14**). Six out of 21 injected animals showed clearly medially ($N = 2$) or laterally ($N = 4$) biased expression. In laterally but not medially biased animals, we noticed dense terminals in the anteroventral periventricular nucleus (AVPV) (**Fig. 8d**). To confirm this result, we injected fluorescently conjugated cholera toxin subunit B

(CTB-555) into AVPV and found that retrogradely labeled cells were largely restricted to the VMHpvll (**Fig. 8e–g**). As a comparison, we injected CTB-555 into the lateral periaqueductal gray (PAG), a region that received comparable projection from the medially and laterally biased animals (**Fig. 8d**), and found the VMHpvlm and VMHpvll to contain similar percentage of CTB-labeled cells (**Fig. 8f,h**). Notably, VMHvl cells retrogradely labeled from either AVPV or PAG overlapped highly with Esr1 (**Fig. 8g**; CTB^+Esr1^+/CTB^+ percentage: from AVPV, 88.5 ± 1.4%; from PAG, 84.1 ± 1.3%; $N = 3$ animals). Finally, consistent with the fact that the AVPV was strongly innervated by mating-related VMHpvll but not by fighting-related VMHpvlm, we found that AVPV expressed high levels of *Fos* after female mating but not fighting (**Fig. 8i,j**). In contrast, the number of fighting- and mating-induced *Fos*-expressing cells was comparable in the lateral PAG (**Fig. 8i,j**).

DISCUSSION

Our study identifies $VMHvl^{Esr1+}$ cells as a neural population that is functionally essential and naturally active during female aggression (**Supplementary Fig. 15a**). Additionally, while in the male VMHvl the fighting and mating related cells overlap substantially[7,36], we found that in the female VMHvl mating and fighting each activate cells that are located in one of the two previously unrecognized subdivisions of the VMHvl (**Supplementary Fig. 15b**).

In two recent studies, the function of the $Esr1^+PR^+$ VMHvl population in female aggression was examined along with its role in male aggression[6,9]. While both studies found a clear role of the $VMHvl^{Esr+PR+}$ population in male aggression, its function in female aggression was unclear. Here we optimized laboratory conditions under which female aggression could be reliably induced. We found that most singly housed SW virgin females readily attacked juvenile intruders, making it possible to study female aggression beyond the lactation period. In addition, by using acute reversible inhibition instead of permanent ablation[9], we minimized changes in female sexual behaviors and avoided possible long-term circuit compensation. We showed in four sets of experiments (**Fig. 3** and **Supplementary Figs. 2** and **6**) that VMHvl activity was necessary for female mouse aggression regardless of the reproductive stage or genetic background of the test females and regardless of the intruder type. While reproductive state, genetic background, housing condition and social experience may fine tune the aggression circuit, the basic circuit wiring is likely to be stable.

Lee *et al.* reported that attack was induced when they activated $VMHvl^{Esr1+}$ cells in C57 males but not virgin C57 females[6]. We repeated this experiment and confirmed that activating the $VMHvl^{Esr1+}$ cells in virgin C57 females did not induce attack but induced male-style mounting. In contrast, when the VMHvl was activated in SW virgin females or C57 lactating females, immediate attack was induced. Notably, in all these optogenetic experiments, the light-induced behavior matched the natural behavior of the test animal: virgin C57 females mount female intruders and never attack any intruder whereas SW virgin females and lactating C57 females attack the intruders and never show any mounting (**Supplementary Table 1**). As shown by our c-Fos mapping and optical recording, the VMHvl is active during both male-style mounting and attack in females. Thus, we speculate that the VMHvl contains populations essential for driving both mounting and fighting in females and, depending on the genetic background and reproductive state of the animals, one population is preferentially activated by the intruder to drive the corresponding behavior. Optogenetic stimulation reactivates the 'dominant' VMHvl population and induces the dominant behavior at the time of stimulation. It is worth noting that male-style mounting behavior is commonly expressed by females in many species. It is believed to play a role in maintaining social dominance[45]. Thus, the mounting in C57 and attacking in SW may be considered different actions for achieving the same goal. Whether it is a mere coincidence or by design that the VMHvl drives both dominance behaviors despite their different motor patterns remains to be elucidated by future studies.

Previous studies showed that low-intensity activation of $VMHvl^{Esr1+}$ cells induces mounting and high-intensity activation induces attack in males[6]. Here we demonstrated that both mounting and attack can be induced in virgin females by activating the $VMHvl^{Esr1+}$ population. Thus, $VMHvl^{Esr1+}$ cells in the female appear to have the capacity to mediate all the social functions ascribed to the corresponding population in males. In addition, the female VMHvl may contain a female-specific population that is specialized for female sexual behaviors (for example, lordosis and ovulation). Our findings reveal that the VMHpvll is largely devoid of aggression-related cells and instead occupied by cells excited during female sexual behaviors. In contrast, the male VMHvl aggression-related and mating-related cells appear to occupy the entire medial–lateral span of the VMHvl (**Supplementary Fig. 15c,d**), leaving little room for cells designated for female-style sexual behavior. Consistent with this hypothesis, the VMHpvll-specific projection to the AVPV is largely absent in male VMHvl (ref. 9), and the VMHpvll-specific gene *Cckar* is minimally expressed in male VMHvl (ref. 46). Perhaps testosterone causes the expansion of the VMHpvlm and shrinkage of the VMHpvll during development and ultimately increases aggression and decreases female-style sexual behaviors in males.

Tinbergen proposed that mating, fighting, parental care and building (a nest) are the four behaviors under the category of reproduction instinct and each of those behaviors (e.g., fighting) contains a series of species-specific consummatory acts (e.g., chasing and biting)[47]. While some social behaviors are qualitatively different between sexes in the sense that males and females express different patterns of consummatory acts, other behaviors may only differ quantitatively. Our results, consistent with previous studies[12,48–50], support common neural substrates for generating qualitatively similar behaviors in males and females whereas sex-specific neural substrates are perhaps reserved for acts (for example, ejaculation and nursing) unique to one sex.

METHODS

Methods, including statements of data availability and any associated accession codes and references, are available in the online version of the paper.

Note: Any Supplementary Information and Source Data files are available in the online version of the paper.

ACKNOWLEDGMENTS

We thank D. Anderson (California Institute of Technology) for providing *Esr1-2A-Cre* mice and B. Lowell (Harvard Medical School) for providing *Vglut2-ires-Cre* and *Vgat-ires-Cre* mice and AAV-DIO-synaptophysin-mCherry for the pilot experiments. We thank R. Machold and M. Baek for technical support on *in situ* hybridization and RNA-seq, C. Loomis at the NYULMC Experimental Pathology Research Laboratory for help on laser capture microdissection, A. Heguy and Y. Zhang at the NYULMC Genome Technology Center for help on RNA-seq and T. Lhakhang at the NYULMC Bioinformatics Laboratory for help with sequence alignment. We thank A.L. Falkner, M. Halassa, G. Stuber and G. Suh for critical comments on the manuscript. This research was supported by a JSPS oversea fellowship (K.H.), Uehara postdoctoral fellowship (K.H.), National Natural Science Foundation of China 81471630 (J.Z.), NIH 1K99NS074077 (H.L.), NIH R21NS093987 (B.R.), NIH P01NS074972 (B.R.), NIH 1R01MH101377

(D. L.), NIH 1R21MH105774-01A1 (D. L.), the Mathers Foundation (D.L.), an Irma T. Hirschl Career Scientist Award (D.L.), a Sloan Research Fellowship (D.L.), a McKnight Scholar Award (D.L.), a Whitehall Fellowship (D.L.) and a Klingenstein Fellowship Award (D.L.).

AUTHOR CONTRIBUTIONS

D.L. supervised the project. D.L. and K.H. conceived the project, designed experiments and wrote the manuscript. K.H. and Y.H. conducted most experiments and analyzed data. R.T. conducted *in vitro* slice physiology. J.Z. conducted pilot pharmacological and c-Fos experiments. J.E.F. optimized *in vivo* single-unit recording. W.T.P. helped with pilot optogenetic experiments. A.S. helped with fiber photometry and optogenetic experiments. H.L. generated Esr1-2A-Cre mice. B.R. supervised slice physiology.

COMPETING FINANCIAL INTERESTS

The authors declare no competing financial interests.

1. Darwin, C. *The Descent of Man, and Selection in Relation to Sex* (D. Appleton and Company, 1871).
2. Lindenfors, P. & Tullberg, B.S. Evolutionary aspects of aggression the importance of sexual selection. *Adv. Genet.* **75**, 7–22 (2011).
3. Kruk, M.R. *et al.* Discriminant analysis of the localization of aggression-inducing electrode placements in the hypothalamus of male rats. *Brain Res.* **260**, 61–79 (1983).
4. Olivier, B. & Wiepkema, P.R. Behaviour changes in mice following electrolytic lesions in the median hypothalamus. *Brain Res.* **65**, 521–524 (1974).
5. Siegel, A., Roeling, T.A.P., Gregg, T.R. & Kruk, M.R. Neuropharmacology of brain-stimulation-evoked aggression. *Neurosci. Biobehav. Rev.* **23**, 359–389 (1999).
6. Lee, H. *et al.* Scalable control of mounting and attack by Esr1+ neurons in the ventromedial hypothalamus. *Nature* **509**, 627–632 (2014).
7. Lin, D. *et al.* Functional identification of an aggression locus in the mouse hypothalamus. *Nature* **470**, 221–226 (2011).
8. Falkner, A.L., Grosenick, L., Davidson, T.J., Deisseroth, K. & Lin, D. Hypothalamic control of male aggression-seeking behavior. *Nat. Neurosci.* **19**, 596–604 (2016).
9. Yang, C.F. *et al.* Sexually dimorphic neurons in the ventromedial hypothalamus govern mating in both sexes and aggression in males. *Cell* **153**, 896–909 (2013).
10. Falkner, A.L., Dollar, P., Perona, P., Anderson, D.J. & Lin, D. Decoding ventromedial hypothalamic neural activity during male mouse aggression. *J. Neurosci.* **34**, 5971–5984 (2014).
11. Falkner, A.L. & Lin, D. Recent advances in understanding the role of the hypothalamic circuit during aggression. *Front. Syst. Neurosci.* **8**, 168 (2014).
12. Kruk, M.R. *et al.* Comparison of aggressive behaviour induced by electrical stimulation in the hypothalamus of male and female rats. *Prog. Brain Res.* **61**, 303–314 (1984).
13. Ogawa, S., Lubahn, D.B., Korach, K.S. & Pfaff, D.W. Behavioral effects of estrogen receptor gene disruption in male mice. *Proc. Natl. Acad. Sci. USA* **94**, 1476–1481 (1997).
14. Spiteri, T. *et al.* The role of the estrogen receptor alpha in the medial amygdala and ventromedial nucleus of the hypothalamus in social recognition, anxiety and aggression. *Behav. Brain Res.* **210**, 211–220 (2010).
15. Sano, K., Tsuda, M.C., Musatov, S., Sakamoto, T. & Ogawa, S. Differential effects of site-specific knockdown of estrogen receptor α in the medial amygdala, medial pre-optic area, and ventromedial nucleus of the hypothalamus on sexual and aggressive behavior of male mice. *Eur. J. Neurosci.* **37**, 1308–1319 (2013).
16. Aou, S., Oomura, Y. & Yoshimatsu, H. Neuron activity of the ventromedial hypothalamus and the medial preoptic area of the female monkey during sexual behavior. *Brain Res.* **455**, 65–71 (1988).
17. Oomura, Y., Aou, S., Koyama, Y., Fujita, I. & Yoshimatsu, H. Central control of sexual behavior. *Brain Res. Bull.* **20**, 863–870 (1988).
18. Pfaff, D.W. & Sakuma, Y. Deficit in the lordosis reflex of female rats caused by lesions in the ventromedial nucleus of the hypothalamus. *J. Physiol. (Lond.)* **288**, 203–210 (1979).
19. Pfaff, D.W. & Sakuma, Y. Facilitation of the lordosis reflex of female rats from the ventromedial nucleus of the hypothalamus. *J. Physiol. (Lond.)* **288**, 189–202 (1979).
20. Musatov, S., Chen, W., Pfaff, D.W., Kaplitt, M.G. & Ogawa, S. RNAi-mediated silencing of estrogen receptor alpha in the ventromedial nucleus of hypothalamus abolishes female sexual behaviors. *Proc. Natl. Acad. Sci. USA* **103**, 10456–10460 (2006).
21. Yang, C.F. & Shah, N.M. Representing sex in the brain, one module at a time. *Neuron* **82**, 261–278 (2014).
22. Bayless, D.W. & Shah, N.M. Genetic dissection of neural circuits underlying sexually dimorphic social behaviours. *Phil. Trans. R. Soc. Lond. B* **371**, 20150109 (2016).
23. Yang, T. & Shah, N.M. Molecular and neural control of sexually dimorphic social behaviors. *Curr. Opin. Neurobiol.* **38**, 89–95 (2016).
24. Lonstein, J.S. & Gammie, S.C. Sensory, hormonal, and neural control of maternal aggression in laboratory rodents. *Neurosci. Biobehav. Rev.* **26**, 869–888 (2002).
25. Parmigiani, S., Palanza, P., Rogers, J. & Ferrari, P.F. Selection, evolution of behavior and animal models in behavioral neuroscience. *Neurosci. Biobehav. Rev.* **23**, 957–969 (1999).
26. Hurst, J.L. & Barnard, C.J. Kinship and social tolerance among female and juvenile wild house mice - kin bias but not kin discrimination. *Behav. Ecol. Sociobiol.* **36**, 333–342 (1995).
27. Koyama, Y., Fujita, I., Aou, S. & Oomura, Y. Proceptive presenting elicited by electrical stimulation of the female monkey hypothalamus. *Brain Res.* **446**, 199–203 (1988).
28. Gunaydin, L.A. *et al.* Natural neural projection dynamics underlying social behavior. *Cell* **157**, 1535–1551 (2014).
29. Cui, G. *et al.* Concurrent activation of striatal direct and indirect pathways during action initiation. *Nature* **494**, 238–242 (2013).
30. Chen, T.W. *et al.* Ultrasensitive fluorescent proteins for imaging neuronal activity. *Nature* **499**, 295–300 (2013).
31. Armbruster, B.N., Li, X., Pausch, M.H., Herlitze, S. & Roth, B.L. Evolving the lock to fit the key to create a family of G protein-coupled receptors potently activated by an inert ligand. *Proc. Natl. Acad. Sci. USA* **104**, 5163–5168 (2007).
32. Dong, S., Rogan, S.C. & Roth, B.L. Directed molecular evolution of DREADDs: a generic approach to creating next-generation RASSLs. *Nat. Protoc.* **5**, 561–573 (2010).
33. Boyden, E.S., Zhang, F., Bamberg, E., Nagel, G. & Deisseroth, K. Millisecond-timescale, genetically targeted optical control of neural activity. *Nat. Neurosci.* **8**, 1263–1268 (2005).
34. Bosch, O.J., Meddle, S.L., Beiderbeck, D.I., Douglas, A.J. & Neumann, I.D. Brain oxytocin correlates with maternal aggression: link to anxiety. *J. Neurosci.* **25**, 6807–6815 (2005).
35. Nomoto, K. & Lima, S.Q. Enhanced male-evoked responses in the ventromedial hypothalamus of sexually receptive female mice. *Curr. Biol.* **25**, 589–594 (2015).
36. Wong, L.C. *et al.* Effective modulation of male aggression through lateral septum to medial hypothalamus projection. *Curr. Biol.* **26**, 593–604 (2016).
37. Guzowski, J.F., McNaughton, B.L., Barnes, C.A. & Worley, P.F. Environment-specific expression of the immediate-early gene Arc in hippocampal neuronal ensembles. *Nat. Neurosci.* **2**, 1120–1124 (1999).
38. Vong, L. *et al.* Leptin action on GABAergic neurons prevents obesity and reduces inhibitory tone to POMC neurons. *Neuron* **71**, 142–154 (2011).
39. Madisen, L. *et al.* A robust and high-throughput Cre reporting and characterization system for the whole mouse brain. *Nat. Neurosci.* **13**, 133–140 (2010).
40. Sapin, E. *et al.* A very large number of GABAergic neurons are activated in the tuberal hypothalamus during paradoxical (REM) sleep hypersomnia. *PLoS One* **5**, e11766 (2010).
41. Jennings, J.H. *et al.* Visualizing hypothalamic network dynamics for appetitive and consummatory behaviors. *Cell* **160**, 516–527 (2015).
42. Lein, E.S. *et al.* Genome-wide atlas of gene expression in the adult mouse brain. *Nature* **445**, 168–176 (2007).
43. Espina, V., Milia, J., Wu, G., Cowherd, S. & Liotta, L.A. Laser capture microdissection. *Methods Mol. Biol.* **319**, 213–229 (2006).
44. Garfield, A.S. *et al.* A neural basis for melanocortin-4 receptor-regulated appetite. *Nat. Neurosci.* **18**, 863–871 (2015).
45. Fang, J. & Clemens, L.G. Contextual determinants of female-female mounting in laboratory rats. *Anim. Behav.* **57**, 545–555 (1999).
46. Xu, X. *et al.* Modular genetic control of sexually dimorphic behaviors. *Cell* **148**, 596–607 (2012).
47. Tinbergen, N. *The Study of Instinct* xii edn., 228 (Clarendon, Oxford, 1951).
48. Unger, E.K. *et al.* Medial amygdalar aromatase neurons regulate aggression in both sexes. *Cell Rep.* **10**, 453–462 (2015).

ONLINE METHODS

Mice and housing. All procedures were approved by the NYULMC IACUC in compliance with NIH guidelines for the care and use of laboratory animals. *Esr1-2A-Cre* knock-in mice[6] were provided by D.J. Anderson and are currently available from Jackson Laboratory (stock no. 017911). They were backcrossed to either SW or C57 for at least five generations. *Vgat-ires-Cre* and *Vglut2-ires-Cre* knock-in mice[38] were provided by B. Lowell and are now commercially available (Jackson Laboratory, stock nos. 016962 and 016963). They were bred to the SW background for over five generations. Ai6 mice[39] were purchased from the Jackson Laboratory (stock no. 007906). Wild-type SW and C57 mice were purchased from Taconic and Charles River, respectively. Mice were housed under a 12 h light-dark cycle (12 p.m. to 12 a.m. light), with food and water available *ad libitum*. All females were group-housed until adulthood. After surgery or 1 week before the resident–intruder test, the test females were singly housed unless they were paired with males or had a litter. Single housing is known to increase aggressiveness in female mice[51], and the reliable expression of aggression was essential for our *in vivo* recording, immediate-early gene mapping and loss-of-function experiments.

Resident–intruder test. To explore behavioral conditions in which female mice show reliable aggression, we tested female aggression in various combinations of subject and intruder types. A juvenile male (C57, 16–25 d old), an adult male (C57, 2–12 months, 18–25 g) or an adult female (C57, 2–12 months, 18–25 g) intruder was introduced into the home cage of a singly housed virgin (2–4 months, SW and C57) or lactating (SW and C57, postpartum days 3–7, 3–5 months) female mouse for 15 min. All test females were singly housed for at least 1 week. All intruder mice were group housed.

Immediate early gene mapping. To induce mating in females, a highly sexually experienced adult male intruder (C57, 4–18 months) was introduced into the home cage of a virgin test female (SW and C57, 2–4 months). Females were only included in the analysis if they showed receptive postures and their male partners achieved intromission. To induce aggression, we used the resident–intruder testing conditions that were effective in eliciting aggression in either virgin or lactating females. Only females that attacked the intruder for at least 5 episodes were included in the analysis. In control group, an object (toy mouse, Zanies) was introduced into the female's cage. To induce fighting and mating in males, an adult group-housed C57 male (2–12 months) or a receptive C57 female (2–4 months) was introduced into the home cage of a singly housed SW male (3–12 months, sexually experienced), respectively. Only males that achieved intromission or attacked the intruder for at least 5 episodes were included in the analysis. The receptivity of the female intruders was determined in advance by behavioral screening using a male mouse different from the testing mouse. For c-Fos immunostaining, each behavioral test lasted 15 min and the animals were perfused 90 min after the test. For catFISH, SW mice experienced two consecutive 5-min behavioral episodes separated by 30 min and were killed immediately after the termination of the second behavioral episode[7].

Video acquisition and behavioral analysis. Animal behaviors in functional manipulation experiments and fiber photometry experiments were video recorded from both the side and the top of the cage using two synchronized cameras (Basler, acA640-100gm) and commercial video acquisition software (StreamPix 5, Norpix) in a semi-dark room with infrared illumination at a frame rate of 25 frames per second. Manual behavioral annotation was performed on a frame-by-frame basis using custom software written in Matlab (https://github.com/pdollar/toolbox/tree/master/videos). Investigation was defined as active nose contact to any part of the body of the intruder or an object by the resident mouse. Attacks were defined by a suite of actions initiated by the resident toward the intruder, which included pushes, lunges, bites, tumbling and fast locomotion episodes between such movements. Mounting refers to the period when the test female was on top of the intruder and held the intruder's lower back using her forelimbs. Being mounted was defined as the behavioral period when the adult male intruder mounted the test female[7].

Fiber photometry recording. The fiber photometry setup was constructed as previously described, with a few modifications[8,28]. A 390-Hz sinusoidal blue LED light (30 μW) (LED light: M470F1; LED driver: LEDD1B; both from Thorlabs) and a 150-Hz sinusoidal yellow LED light nm (30 μW) (Thorlabs, M590F1) were bandpass filtered (passing band: 472 ± 15 nm, FF02-472/30-25; 590 ± 20 nm, FF01-590/20-25, Semrock) and delivered to the brain to excite GCaMP6f and mCherry, respectively. The emission light traveling back through the same optic fiber and was bandpass filtered (passing bands: 524 ± 29 nm and 628 ± 33 nm, FF01-524/628-25, Semrock) and detected by a femtowatt silicon photoreceiver (Newport, 2151) and recorded using a real-time processor (RP2, Tucker Davis Technology (TDT)). The envelopes of the 390-Hz and 150-Hz signals reflected the respective intensity of the GCaMP and mCherry and were extracted in real time using a custom TDT program.

AAV1-CAG-Flex-GCaMP6f (100 nl, 2.0×10^{12} vg/ml; University of Pennsylvania Vector Core facility) was stereotactically injected into the unilateral VMHvl through a glass capillary using a nanoinjector (World Precision Instruments, Nanoliter 2000) at 15 nl/min. A similar injection procedure was used in all functional experiments. After injection, a custom-made optic fiber assembly (Thorlabs, BFH48-400 and CF440-10) was inserted ~100 μm above the VMHvl of *Esr1-2A-Cre* mice (2–4 months old) and was secured using dental cement (C&B Metabond, S380). The coordinates for targeting the VMHvl (from bregma, AP: −1.7, ML: ±0.67, DV: −5.68 mm) were determined from a three-dimensional fMRI mouse atlas[52]. To estimate the distribution of recorded cells, we analyzed the location of cells underneath the putative light core (angle 28°) from the optic fiber (NA 0.48). All virgin mice were singly housed after the surgery and during the tests. For experiments using lactating females, female mice were paired with an adult male mouse 1 week after surgery and were housed together until midterm pregnancy. Pups were separated from lactating female mice 5 min before the tests.

The optical recording was performed 3–6 weeks after viral incubation. Before recording, pups, if any, were removed. During recording, a juvenile male (16–25 d), an adult C57 male (>2 months) and an object (toy mouse, Zanies) were introduced into the cage of the subject female in a randomized order. Some animals were also tested with pups (day 2 to 7) and adult female intruders (>2 months). Each stimulus was presented for 15 to 20 min and at least twice. Five-minute intervals were given between each stimulus presentation. To examine neural response to olfactory cues from conspecifics (**supplementary Fig. 3**), urine from adult C57 males or juvenile males was collected onto a cotton tip and was presented in front of the nose of the subject female mice in their home cages 4–6 times.

To account for the autofluorescence from the system and the brain, we measured fluorescence intensity of each mouse on the day after the surgery. This value was later subtracted from the GCaMP6 signal obtained during the actual experiments. The normalized fluorescence signals (Fn) during each stimulus presentation were obtained by dividing the adjusted raw GCaMP6 signal by the mean fluorescence value from 100 s to 0 s before the stimulus introduction. In **Figure 2d** (left), the subject's location was tracked using a custom-written Matlab program[7,53]. The velocity was calculated as the difference in the animal's location between the current frame and the previous frame. The average GCaMP6f signal and the average velocity at each second throughout the recording were calculated to construct the scatter plot in **Figure 2d**. In **Figure 2d–i,l–n**, the onset/offset peri-event time histograms (PETHs) were constructed by first calculating the average raw GCaMP6 signal aligned to the onset and offset of the behavioral events, and then normalized by calculating $(F - F_{baseline})/F_{baseline}$. $F_{baseline}$ was the average signal between −5 s and −3 s from the onset of the behavior. We did not use the period immediately before the behavioral onset as the baseline given that the GCaMP6 signal may start to increase before the behavioral onset. In **Figure 2j–l,n**, peak $\Delta F/F$ was defined as the maximum $\Delta F/F$ of the PETHs within 2 s after behavioral onset minus the maximum $\Delta F/F$ between −5 and −3 s before the behavioral onset. In **Figure 2m**, offset peak $\Delta F/F$ was defined as the maximum $\Delta F/F$ of the PETHs within 2 s before behavioral offset minus the maximum $\Delta F/F$ between −5 and −3 s before the behavioral onset.

hM4Di-mediated neural silencing. For silencing VMHvl neurons in wild-type SW female mice (3–5 months), a mixture of AAV2-hSyn-DIO-hM4Di-mCherry (5.8×10^{12} vg/ml, UNC Vector Core) and AAV2-CMV-Cre (3.7×10^{13} vg/ml, University of Iowa Vector Core facility) in a 2:1 volume ratio was prepared. Control virus was a mixture of AAV2-hSyn-DIO-mCherry (2.0×10^{12} vg/ml, UNC Vector Core) and AAV2-CMV-Cre (3.7×10^{13} vg/ml, University of Iowa Vector Core facility) in a 2:1 volume ratio. Mice were bilaterally and stereotactically injected with a total of 350 nl of the mixed viruses on each side. Seven days

doi:10.1038/nn.4644

after the injection, each female mouse was paired with a male mouse until the female became visibly pregnant. From postpartum day 2 to day 7, mice in the test group were intraperitoneally injected with saline or CNO (0.5 mg/kg, Sigma, C0832) on interleaved days. Thirty minutes after injection, pups were removed from the female's cage and 2 min later a randomly selected, group-housed adult C57 male intruder (18–25 g) was introduced for approximately 10 min to evaluate the aggression level of the female. After the intruder mouse was removed from the cage, four pups were introduced into the furthest corner from the nest and the amount of time to retrieve all the pups back to the nest was recorded as an index of pup retrieval performance.

To silence the Esr1$^+$ population in VMHvl, we injected 140 nl per side of AAV1-Ef1α-DIO-hM4Di-mCherry (3.0×10^{12} vg/ml, UNC Vector Core) bilaterally into the VMHvl of *Esr1-2A-Cre* mice (either SW background or C57 background, 3–5 months). Control animals were of the same genetic background and were injected with 140 nl per side AAV2-hSyn-DIO-mCherry (3.0×10^{12} vg/ml, UNC Vector Core). Surgical and behavioral testing procedures were similar to those used for wild-type mice, with two differences. First, test animals were split into two groups. One group received saline injection on the first testing day and the second group received CNO injection on the first testing day. This counterbalanced procedure ensured that any observed changes in aggression were not due to natural fluctuation in aggression across postpartum days. Second, each female was tested first with a juvenile male mouse intruder (16–25 d) and then with an adult male mouse intruder. In addition to testing lactating subjects, the behavioral effects of silencing the Esr1$^+$ population in the VMHvl of virgin female mice were also tested. Virgin SW *Esr1-2A-Cre* mice were injected with 140 nl per side of AAV1-Ef1α-DIO-hM4Di-mCherry (3.0×10^{12} vg/ml, UNC Vector Core) bilaterally into the VMHvl. Three weeks after the injection, they received saline and CNO (0.5 mg/kg, Sigma, C0832) on 6 interleaved days 30 min before the aggression test with a juvenile male intruder.

For behavioral analysis, all animals with >10% VMHvl cells expressing hM4Di-mCherry were included. To compare the aggression levels after CNO and saline injections, data for each animal from all CNO-injected days were combined and data from all saline-injected days were combined, given that no significant differences in behaviors were found across CNO days or across saline days. The shortest durations to retrieve all four pups among all saline days and among all CNO days were used for comparing the performance in pup retrieval. The correlation between the number of infected cells and the behavioral changes was examined using all animals with average attack duration on saline days over 20 s.

ChR2 mediated cell activation. For activating VMHvl^{Esr1+} neurons, we stereotactically injected 100 nl of AAV2-Ef1α -DIO-ChR2-EYFP (2×10^{12} vg/ml, UNC Vector Core) bilaterally into the VMHvl of virgin SW or C57 *Esr1-2A-Cre* mice (3–5 months). The control females were injected with AAV2-hSyn-DIO-mCherry (3.0×10^{12} vg/ml, UNC Vector Core). Immediately after viral injection, a bilateral guide cannula (Plastics One, center-to-center distance 1.5 mm) was inserted 0.7 mm above the target area and was secured using dental cement (C&B Metabond, S380).

After 2 weeks of viral incubation, on the test days, two 230-μm multimode optical fibers (Thorlabs) were inserted into the bilateral guide cannula (Plastics One) and secured with a matching cap (Plastics One). The optic fiber ends were flush with the cannula ends. Randomly selected group-housed adult C57 male or female mice (>2 months) were introduced into the subject's home cage, one at a time and each for 30–90 min. Blue light (473 nm, Shanghai Dream Laser) was delivered through the fiber unilaterally in 20-ms pulses at 20 Hz with the intensity ranging from 0.02 to 3 mW for 60 s. The light intensity was measured at the fiber end during pulsing using an optical power meter (Thorlabs, PM100D). A sham stimulation period (0 mW) was interleaved with the real light stimulation period as an internal control. All behavioral tests were repeated at least once to ensure the reproducibility of any light-induced behavioral changes. Mice were killed within 30 d of viral injection so that ChR2-EYFP expressing cells could be counted. Over time, EYFP expression increases in the cell membrane, which makes the counting less reliable.

For activating the Esr1$^+$ population in the VMHvl of *Esr1-2A-Cre* lactating mice with a C57 background (3–5 months), 100 nl of AAV2-Ef1α-DIO-ChR2-EYFP (2×10^{12} vg/ml, UNC Vector Core) was bilaterally injected. One week after injection, each female was paired with an adult C57 male (3–12 months). Once the female became visibly pregnancy, the male was removed. On postpartum day 2, the lactating female was first tested in a resident–intruder assay against a juvenile intruder. If the female showed any attack, we then tested for light-induced behavioral changes using the same stimulation protocol described above.

To confirm the efficacy of ChR2 stimulation in inducing neural activation, blue light (20 ms, 20 Hz, 1–2 mW, seven times, 40 s on and 20 s off) was delivered in the absence of any intruder 90 min before killing the animals. The light intensity was the same as that optimized for eliciting attack on previous testing days. Non-attackers and control animals expressing only mCherry were stimulated with the same protocol at 1.5 mW. The neural activation was then assessed by c-Fos staining. For behavioral analysis, all animals with >10% VMHvl cells expressing light-induced c-Fos in either anterior (from bregma: −1.4 mm) or posterior (from bregma: −1.6 to −2.0 mm) VMHvl were included.

Tracing. To investigate downstream targets of VMHvl^{Esr1+} cells, 15 nl of AAV9-Ef1α-DIO-synaptophysin-mCherry (1.0×10^{13} vg/ml, MIT Viral Core) was stereotactically injected unilaterally into the VMHvl of virgin *Esr1-2A-Cre* SW females (2–5 months). Four weeks after injection, animals were killed for histological analysis. To label VMHvl neurons that project to AVPV or PAG, the retrograde tracer cholera toxin subunit B conjugated to Alexa Fluor 488 or 555 (CTB-488 or CTB-555, 1 mg/ml, ThermoFisher) was injected unilaterally into AVPV (0.07 mm, 0.1 mm, 4.75 and 5.05 mm; 60 nl in each site) or lateral PAG (0.25 mm, −4.5 mm, −1.9 mm and 0.29 mm, −4.8 mm, −1.8 mm; 80 nl in each site). Seven days after surgery, animals were sacrificed for histological analysis, which included Esr1 and fluorescent Nissl staining. As we observed no difference in the labeling pattern at the VMHvl between CTB-488 and CTB-555 injected animals, data from these two tracers were pooled for final analysis.

Immunohistochemistry. For detection of c-Fos and/or viral expression in wild-type mice, frozen sections were prepared. Animals were deeply anesthetized with a mixture of ketamine (100 mg/kg) and xylazine (10 mg/kg) and transcardially perfused with 20 ml of PBS, followed by 20 ml of 4% paraformaldehyde (PFA, Sigma) in PBS. After perfusion, brains were extracted, soaked in 20% of sucrose in PBS for 24 h at 4 °C and then embedded with O.C.T compound (Fisher Healthcare). Coronal brain sections 25 μm (**Fig. 7d**,**e** and **Supplementary Figs. 1**, **12** and **15**) or 35 μm (**Supplementary Fig. 2**) thick were cut using a cryostat (Leica). Brain sections were washed with PBS (once for 10 min) and PBST (0.1% Triton X-100 in PBS, once for 10 min), blocked in 10% normal donkey serum (NDS) in PBST for 30 min at room temperature, and then incubated with primary antibodies in 1% NDS in PBST overnight at 4 °C. Sections were then washed with PBST (three times for 5 min each), incubated with secondary antibodies in 1% NDS in PBST for 2 h at room temperature, washed with PBST (twice for 10 min each), counterstained with DAPI (Sigma), and finally washed again with PBS (twice for 10 min each). Slides were coverslipped using mounting medium (Vectashield, H1000).

For the experiments with a need to analyze Esr1 expression, fresh floating sections were prepared. Animals were deeply anesthetized with a mixture of ketamine (100 mg/kg) and xylazine (10 mg/kg) and transcardially perfused with 20 ml of PBS, followed by 40 ml of 4% PFA. Brains were postfixed for 1–2 h in 4% PFA and transferred to PBS with 0.05% sodium azide (Sigma) at 4 °C until sectioning. Coronal sections 40–60 μm thick were obtained using a vibratome (Leica, VT1200). Sections were stored in PBS with 0.05% sodium azide at 4 °C until use. Sections were washed with PBS (three times for 5 min each) and then blocked in 10% NDS in PBST (0.3% Triton) for 2 h at room temperature, followed by incubation with primary antibodies in 10% NDS in PBST (0.3% Triton) for 72 h at 4 °C. Sections were washed with PBST (0.3% Triton, three times for 30 min each), incubated with secondary antibodies in 10% NDS in PBST (0.3% Triton) and NeuroTrace 435/455 blue fluorescent Nissl stain (Life Technologies, 1:200) for 2 h at room temperature, washed with PBST (twice for 15 min each) and PBS (twice for 15 min each), mounted on slides and coverslipped with mounting medium.

The primary antibodies used were rabbit anti-Esr1 (1:500, Santa Cruz, sc-542, lot F1715; nonspecific staining was occasionally observed using other lots) and goat anti-c-Fos (1:200, Santa Cruz, sc52-g). The secondary antibodies used were donkey anti-rabbit Alexa 488 (1:500, Life Technologies, A21206), donkey anti-rabbit Alexa 546 (1:500, Life Technologies, A10040), donkey anti-rabbit Alexa 594 (1:500, Life Technologies, A21207), donkey anti-goat Alexa 488 (1:500, Life Technologies, A11055), donkey anti-goat Alexa 594 (1:500, Life Technologies,

A11058), donkey anti-goat Alexa 633 (1:500, Life Technologies, A21082) and donkey anti-goat Cy5 (1:300, Jackson ImmunoResearch, 705-175-147).

Fluorescence *in situ* hybridization. For detecting *Fos,* flash-frozen sections were prepared. Briefly, mice were anesthetized immediately after the 5-min behavioral episode using isoflurane and decapitated. Brains were transferred to a beaker containing ice-cold 2-methylbutane (Sigma) and then the beaker was moved to an ethanol and dry ice mixture to quickly freeze the brains. The brains were frozen within 2 min after the termination of the behavior and then stored at −80 °C until sectioning.

Fluorescence *in situ* hybridization (FISH) was used to detect *Fos*. As described previously[7], a 2,4-dinitrophenol (DNP)-labeled *Fos* RNA probe and a digoxigenin (DIG)-labeled *Fos* intronic RNA probe were synthesized using cDNAs with T7 polymerase (Roche). Hybridization was conducted with 1–2 ng/µl RNA probes at 56 °C for 16 h. Probe detection was performed using horseradish peroxidase–conjugated antibodies (PerkinElmer). Signals for DIG-labeled probes were further amplified using biotin-conjugated tyramide (PerkinElmer) that was subsequently visualized with Alexa 555-conjugated streptavidin (Life Technologies). Signals for DNP-labeled probes were amplified using DNP-conjugated tyramide (PerkinElmer) that was subsequently detected with anti-DNP Alexa 488 (Life Technologies). Sections were counterstained with Hoechst (1:2,000, Life Technologies).

For visualizing mRNAs except for *Fos,* fixed sections were prepared. Mice were deeply anesthetized with a mixture of ketamine (100 mg/kg) and xylazine (10 mg/kg) and transcardially perfused with 20 ml of PBS, followed by 40 ml of 4% PFA in PBS. After perfusion, brains were extracted, soaked in 20% sucrose in PBS for 24 h at 4 °C and then embedded with O.C.T compound. Coronal sections 20 µm thick were obtained using a cryostat and mounted on slides. Slides were stored at −80 °C until use.

RNA probes for *Tac1*, *Egflam*, *Crhbp*, *Cckar* and *Iigp1* were designed following the Allen Brain Atlas's probe design guideline (http://help.brain-map.org/display/mousebrain/Documentation?preview=/2818169/3276841/ABADataProductionProcesses.pdf). Briefly, transcript sequences of target genes were analyzed with BLAST and high-homology regions were detected. Primers were designed with Primer-BLAST according to the guideline's criteria, avoiding the high homology region; primer size 20–24 nt; GC content 42–52%; final product size 300–1,200 nt. DNA templates for riboprobe *in vitro* transcription were generated by PCR using both cDNA clones and genomic DNA (**Supplementary Data Set 2**). For genomic DNA, nested PCR was performed. For each target gene, three or four DIG-labeled probes were produced and mixed.

For genes except for *Fos*, chromogenic *in situ* hybridization (CISH) was performed. Hybridization was performed with DIG-labeled riboprobes (1–2 ng/µl) at 56 °C for 16 h. Probe detection was performed using horseradish peroxidase–conjugated antibodies (PerkinElmer). Signals for DIG-labeled probes were amplified using biotin-conjugated tyramide (PerkinElmer), followed by streptavidin–alkaline phosphatase reaction, and then detected by NBT (nitro blue tetrazolium chloride, Sigma) and BCIP (5-bromo-4-chloro-3-indolyl phosphate, toluidine salt, Sigma).

Image acquisition. Tiled confocal images were acquired with 2 µm optical thickness using 20× or 40× objectives (Zeiss LSM 510 or 700 microscope). The image acquisition settings were maintained for each experiment. *z*-stacks were acquired for quantifying ChR2-EYFP and *Fos* in catFISH experiments. Epifluorescence images were acquired for determining electrode location in **Figure 5** (Zeiss Axio). Bright-field images were acquired for CISH experiments in **Figure 7** (Olympus AX70). ImageJ or Neurolucida (MBF Bioscience) was used to quantify the staining results by an observer blind to the experimental conditions.

Electrophysiological recordings of acute slices. A mixture of AAV1-Ef1α-DIO-hM4Di-mCherry (3.0×10^{12} vg/ml, UNC Vector Core) and AAV2-CMV-Cre (1.1×10^{14} vg/ml, University of Iowa Vector Core facility) was stereotactically injected into the VMHvl of virgin wild-type SW female mice (3–4 weeks). AAV1-Ef1α-DIO-hM4Di-mCherry (100 nl, 3.0×10^{12} vg/ml, UNC Vector Core) was stereotactically injected into the VMHvl of virgin *Esr1-2A-Cre* SW female mice (3–4 weeks). After 3 weeks of viral incubation, mice were anesthetized with intraperitoneal injection of pentobarbital (100 mg/kg body weight). Upon loss of reflexes, mice were transcardially perfused with ice-cold oxygenated ACSF containing the following (in mM): 87 NaCl, 75 sucrose, 2.5 KCl, 1.25 NaH_2PO_4, 26 $NaHCO_3$ 10 glucose, 1 $CaCl_2$ and 2 $MgCl_2$. Mice were then decapitated and 300-µm-thick coronal slices were sectioned using a Leica VT-1200-S vibratome and incubated in a holding chamber at 32–35 °C for 15–30 min followed by continued incubation at room temperature for at least 45–60 min before physiological recordings. A slice containing VMHvl was then transferred into a recording chamber and submerged in oxygenated ACSF containing the following (in mM): 125 NaCl, 2.5 KCl, 1.25 NaH_2PO_4, 26 $NaHCO_3$, 10 glucose, 2 $CaCl_2$ and 1 $MgCl_2$ (pH 7.4, bubbled with 95% O_2 and 5% CO_2), in addition to 10 µM CNQX, 25 µM AP-5 and 10 µM SR-95531 to block AMPA, NMDA and $GABA_A$ receptors, respectively. ACSF was perfused through the chamber (~5 mL/min, 34 °C) throughout the experiment. Whole-cell current-clamp recordings were obtained from visually identified mCherry-expressing cells using borosilicate pipettes (3–5 M) containing the following (in mM): 130 potassium gluconate, 6.3 KCl, 0.5 EGTA, 10 HEPES, 4 Mg-ATP, 0.3 Na-GTP (pH adjusted to 7.3 with KOH). Upon break-in, series resistance (typically 15–25 M) was compensated and only stable recordings (<20% change) were included. Data were acquired using an Axopatch 700B amplifier, sampled at 20 kHz and filtered at 10 kHz. Since resting membrane potential was variable from cell to cell and some cells were spontaneously active, all cells were held at −60 mV with a DC current and current-step protocols applied to extract basic sub- and suprathreshold electrophysiological properties such as input resistance and action potential threshold. The DC current was then removed and 10 µM CNO was applied. After at least 5 min of CNO application, cells were again held at −60 mV and intrinsic properties were reassessed using the same protocols as before CNO application. Data were analyzed off-line using Clampfit 10.2 software (Molecular Devises).

***In vivo* electrophysiological recordings.** The recording procedures were described previously[7]. Adult virgin SW females (3–6 months) were used for recording. The electrode was composed of sixteen 13-µm tungsten wires (California Fine Wires, part no. M281770), each attached to a pin on a nanoconnector (Omnetics, no. 1619). The electrode assemble was glued to a movable aluminum block driven by a 00-90 screw (J.J. Morris) on a custom-made microdriver. Each turn of the screw advances the electrode by 280 µm. During surgery, three anchor screws (J.J. Morris, part no. F000CE094) were drilled into the skull. The electrode was then lowered right above the VMHvl (depth: 5.4 mm) and the microdriver was secured to the skull and anchor screws using dental cement. After 1 week of recovery, on the days of recording, the electrode was connected to a chronic headstage (TDT, LP16CH) that was connected to a torqueless, feedback-controlled commutator (TDT, AC32). The headstage was further connected to a 16-channel preamplifier (TDT, RA16PA) and recorded with a real-time digital processor (TDT, RZ5). Signals from electrodes were band-pass filtered from 300 Hz to 3,000 Hz. Each video frame acquisition was triggered by a TTL pulse from the recording setup to ensure synchronization between the video and the electrophysiological recording.

During recording, a juvenile male, a juvenile female, an adult C57male, an adult SW male or a toy mouse was introduced into the cage of the recorded female in a randomized order each for approximately 5 min and with 5 min in between. Each stimulus was introduced at least twice to test the reproducibility of cell responses. Each day, the entire recording was broken into two to four recording blocks, each for approximately 1 h. The first 5 min of each block was used as the baseline period and no stimulus was presented during that period. After each recording session, the electrode bundle was advanced by one-eighth turn. After approximately 10 recording sessions in each subject, mice were killed and histological analyses were performed to verify the locations of the electrodes. Only animals with successful targeting of the VMHvl were included in the final analysis.

Spike sorting was performed using Offline Sorter (Plexon). Individual units recorded from the same electrode were isolated using principal component analysis. Three criteria were imposed for identifying single units: (i) signal to noise ratio was above 3, (ii) the waveform of the spikes was stable in the entire recording session, and (iii) spikes with inter-spike intervals below 3 ms made up no more than 0.1%. Only units meeting all three criteria were included in the final analysis. To analyze the firing rate during each behavior, we sequentially combined all spikes occurred during a specific behavior and then calculated the number of spikes in each 1-s bin during the behavior. We then compared the firing rates during a behavior and that during the baseline period using a *t*-test for

 doi:10.1038/nn.4644

each unit. Units were regarded as responsive to a social stimulus if (i) the firing rate during investigation of a social stimulus was significantly higher than that during baseline (t-test, $P < 0.01$) and (ii) the significant response was repeatable. Across all 20 recording sessions, the duration of the baseline was 448 ± 19.8 s. The durations investigating a juvenile male and an adult C57 male were 111 ± 7.47 s and 65.2 ± 4.99 s, respectively.

We constructed the PETHs (±5-s window, 250-ms bin) aligned to the onset of investigating or attacking a juvenile for juvenile-excited cell with at least 3 s of each analyzed behavior. We constructed the PETHs aligned to the onset of investigating and being mounted by a male for adult-male-excited cell with at least 3 s of these two behaviors. Eighteen of 22 juvenile-excited cells and 9 of 27 male-excited cells met these criteria and were used to construct the population PETHs in **Figure 5b** and **Figure 5e**, respectively.

LCM–RNA-seq. Three group-housed adult *Vglut2-ires-Cre* × Ai6 female mice (10–12 weeks) were decapitated. The brains were flash frozen within 2 min and stored at −80 °C until sectioning. Coronal sections 20 µm thick were obtained using a cryostat and mounted on slides that were dehydrated in 100% ethanol for 1 min and then dried by using a hair dryer. Slides were stored at −80 °C until use. Given that VMH is composed largely of glutamatergic cells that are surrounded by GABAergic cells and each subdivision of VMH has a cell-poor boundary, the ZsGreen labeling in glutamatergic cells enabled recognition of the subdivisions. The anterior one-third of the VMHvl was regarded as VMHavl while the remaining VMHvl was regarded as posterior VMHvl. VMHdm, VMHavl, VMHpvlm and VMHpvll were laser-dissected using a LMD6000 (Leica) fluorescence microscope combined with a movable laser for microdissection. Collected tissues were lysed in extraction buffer and total RNA was isolated using a PicoPure RNA isolation kit (ThermoFisher). The RNA-seq libraries were then prepared using Clontech SMARTer Stranded Total RNA-Seq Kit (cat. no. 635006) and purified using AMPure beads (Beckman Coulter). The quantity of the library was examined using Qubit RNA HS assay Kit (Thermo Fisher Scientific) and qPCR. The quality of the library was determined using Bioanalyzer (Agilent). Once the libraries were deemed high quality (free of adaptor dimers and in concentration >2 nM), we pooled eight samples equimolarly and sequenced them by Illumina HiSeq 2500 using high output mode to achieve greater depth of coverage. Read alignment was carried out using HISAT2 (https://github.com/infphilo/hisat2) against the mouse mm10 reference genome obtained from Ensembl database (http://ensembl.org/). The alignment results were then exported to the open-source software Featurecounts to determine the number of reads for each gene. Then the Bioconductor software package DESeq2 was used to identify genes that were differentially expressed across VMH subregions (adjusted $P < 0.05$). Among those significantly differentially expressed genes, we selected a subset of pvlm- and pvll-specific genes with moderate to high levels of expression (pvlm-specific: pvlm/pvll > 1.2 and pvlm normalized counts > 4 at $\log_2$ scale; pvll-specific: pvll/pvlm > 1.2 and pvlm normalized counts > 4 at $\log_2$ scale) and conducted *in situ* hybridization of each gene to visualize its expression pattern in the VMH.

Statistical analysis. Statistical analyses were performed using Matlab or Prism software (GraphPad). All statistical analyses were two-tailed. Comparisons between two groups were performed by unpaired or paired t-test. Comparisons among three or more groups were performed using ANOVA. *Post hoc* multiple comparisons were done using the Holm–Sidak test for paired data and Tukey test for unpaired data. All significant statistical results are indicated on the figures with the following conventions: $^{*}P < 0.05$, $^{**}P < 0.01$, $^{***}P < 0.001$. Error bars represent ± s.e.m.

No statistical methods were used to predetermine the sample sizes, but our sample sizes are similar to those generally employed in the field. Data distribution was assumed to be normal, but this was not formally tested. Cell count, anatomical and behavioral analysis were fully and/or partially conducted by experimenters blind to experimental conditions. A **Life Sciences Reporting Summary** is available.

Data availability. The data that support the findings of this study are available from the corresponding author upon reasonable request. The RNA-seq data are available from NIH GEO: GSE103183.

Code availability. The code used to analyze data and generate figures in this study is available from the corresponding author upon reasonable request.

49. Wu, Z., Autry, A.E., Bergan, J.F., Watabe-Uchida, M. & Dulac, C.G. Galanin neurons in the medial preoptic area govern parental behaviour. *Nature* **509**, 325–330 (2014).
50. Kimchi, T., Xu, J. & Dulac, C. A functional circuit underlying male sexual behaviour in the female mouse brain. *Nature* **448**, 1009–1014 (2007).
51. Kuchiiwa, S. & Kuchiiwa, T. A novel semi-automated apparatus for measurement of aggressive biting behavior in mice. *J. Neurosci. Methods* **228**, 27–34 (2014).
52. Chan, E., Kovacevíc, N., Ho, S.K., Henkelman, R.M. & Henderson, J.T. Development of a high resolution three-dimensional surgical atlas of the murine head for strains 129S1/SvImJ and C57Bl/6J using magnetic resonance imaging and micro-computed tomography. *Neuroscience* **144**, 604–615 (2007).
53. Wang, L., Chen, I.Z. & Lin, D. Collateral pathways from the ventromedial hypothalamus mediate defensive behaviors. *Neuron* **85**, 1344–1358 (2015).

nature research

Corresponding author(s): Dayu Lin

☐ Initial submission ☐ Revised version ☒ Final submission

Life Sciences Reporting Summary

Nature Research wishes to improve the reproducibility of the work that we publish. This form is intended for publication with all accepted life science papers and provides structure for consistency and transparency in reporting. Every life science submission will use this form; some list items might not apply to an individual manuscript, but all fields must be completed for clarity.

For further information on the points included in this form, see Reporting Life Sciences Research. For further information on Nature Research policies, including our data availability policy, see Authors & Referees and the Editorial Policy Checklist.

Experimental design

1. Sample size

Describe how sample size was determined.

We did not do any statistical tests to predetermine the sample size.
For behavioral, imaging, and staining experiments, n>3 for each group. Sample sizes were reported in figure legends and method.

2. Data exclusions

Describe any data exclusions.

Yes, in DREAD experiments, we excluded animals with minimal infection (<10%) from analysis except for correlation data.
This criteria was established before data collection.

3. Replication

Describe whether the experimental findings were reliably reproduced.

All the experiments have biological replicates that support our conclusion.
Individual data is presented for transparency.

4. Randomization

Describe how samples/organisms/participants were allocated into experimental groups.

Test and control groups were conducted at the same time by assigning samples to each group randomly.

5. Blinding

Describe whether the investigators were blinded to group allocation during data collection and/or analysis.

Cell count, anatomical and behavioral analysis were fully and/or partially conducted by experimenters blind to experimental conditions.

Note: all studies involving animals and/or human research participants must disclose whether blinding and randomization were used.

6. Statistical parameters

For all figures and tables that use statistical methods, confirm that the following items are present in relevant figure legends (or in the Methods section if additional space is needed).

n/a	Confirmed	
☐	☒	The exact sample size (*n*) for each experimental group/condition, given as a discrete number and unit of measurement (animals, litters, cultures, etc.)
☐	☒	A description of how samples were collected, noting whether measurements were taken from distinct samples or whether the same sample was measured repeatedly
☐	☒	A statement indicating how many times each experiment was replicated
☐	☒	The statistical test(s) used and whether they are one- or two-sided (note: only common tests should be described solely by name; more complex techniques should be described in the Methods section)
☐	☒	A description of any assumptions or corrections, such as an adjustment for multiple comparisons
☐	☒	The test results (e.g. *P* values) given as exact values whenever possible and with confidence intervals noted
☐	☒	A clear description of statistics including central tendency (e.g. median, mean) and variation (e.g. standard deviation, interquartile range)
☐	☒	Clearly defined error bars

See the web collection on statistics for biologists for further resources and guidance.

Nature Neuroscience: doi:10.1038/nn.4644

Software

Policy information about availability of computer code

7. Software

Describe the software used to analyze the data in this study.	http://vision.ucsd.edu/~pdollar/toolbox/doc/index.html for behavioral annotation This software was used throughout the study to classify observed behaviors.

For manuscripts utilizing custom algorithms or software that are central to the paper but not yet described in the published literature, software must be made available to editors and reviewers upon request. We strongly encourage code deposition in a community repository (e.g. GitHub). *Nature Methods* guidance for providing algorithms and software for publication provides further information on this topic.

Materials and reagents

Policy information about availability of materials

8. Materials availability

Indicate whether there are restrictions on availability of unique materials or if these materials are only available for distribution by a for-profit company.	We used commercially available materials throughout the study. The vendor is stated for each item in Method.

9. Antibodies

Describe the antibodies used and how they were validated for use in the system under study (i.e. assay and species).	http://www.scbt.com/datasheet-52-c-fos-4-antibody.html http://www.scbt.com/datasheet-542-eralpha-mc-20-antibody.html These antibodies were widely used for detection of fos or Esr1. We also conducted pilots experiments to optimize staining conditions.

10. Eukaryotic cell lines

a. State the source of each eukaryotic cell line used.	n.a.
b. Describe the method of cell line authentication used.	n.a.
c. Report whether the cell lines were tested for mycoplasma contamination.	n.a.
d. If any of the cell lines used are listed in the database of commonly misidentified cell lines maintained by ICLAC, provide a scientific rationale for their use.	n.a.

Animals and human research participants

Policy information about studies involving animals; when reporting animal research, follow the ARRIVE guidelines

11. Description of research animals

Provide details on animals and/or animal-derived materials used in the study.	Esr1-2A-Cre knock-in mice with SW or C57 background were used (provided by D. Anderson; Jackson Laboratory, stock No. 017911). Vgat-ires-Cre and Vglut2-ires-Cre knock-in mice with SW background were used (provided by B. Lowell; Jackson Laboratory, stock No: 016962 and 016963).Ai6 was used to generate reporter mice (Jackson Laboratory,Stock No.007906). Wild-type SW and C57 mice were also used.

Policy information about studies involving human research participants

12. Description of human research participants

Describe the covariate-relevant population characteristics of the human research participants.	n.a.

Nature Neuroscience: doi:10.1038/nn.4644